RESTRAINED SHRINKAGE BEHAVIOR OF HIGH PERFORMANCE CONCRETE REINFORCED WITH HYBRID FIBERS

By

MINA HABIB

A thesis submitted to the

School of Graduate Studies

Rutgers, the State University of New Jersey

In Partial Fulfillment of the requirements

For the degree of

Master of Science

Graduate Program in Civil and Environmental Engineering

Written under the direction of

Dr. Hani H. Nassif

And Approved By

_____

_____

_____

New Brunswick, New Jersey

May 2019

ABSTRACT OF THESIS

RESTRAINED SHRINKAGE BEHAVOR OF HIGH PERFORMANCE CONCRETE REINFORCED WITH HYBRID FIBERS

By MINA HABIB

Thesis Director: Dr. Hani H. Nassif

High-performance concrete (HPC) is characterized as a type of concrete that has superior strength and durability than typical Class A concrete. These qualities are what makes its application very common in slab-on-girder bridges. A stronger concrete mix will have a higher tensile strength, one that requires a higher tensile strain to induce cracking. Although HPC has higher strength than typical Class A concrete, it is still susceptible to cracking due to different types of shrinkage. There are ways to combat this shrinkage, some of which include, but are not limited to, utilizing shrinkage-reducing admixtures, wet-curing, and implementing fibers into the mix design. Fiber-reinforced concrete is being implemented in structures all over the world, and its practice in the industry is more possible than ever due to the introduction of high-range water reducing admixtures.

Fibers are added to concrete for a plethora of reasons, some of which are highly favorable in particular circumstances. The natural brittle tendency of concrete is a common concern among designers, and adding fibers into their mix design increases tensile strength by mitigating crack propagation. Once a concrete member is subjected to

tensile stress, the fibers distributed among the member will intercept the cracks as they are made and as they grow in depth and width.

Even if a concrete element is designed to be in compression, tensile stresses can still be induced as a result of restrained shrinkage. In bridge decks, the bottom surface of the slab is typically held in place by a steel deck, while the top surface remains exposed. This differential drying shrinkage induces tensile stresses that eventually lead to transverse cracking. As deicing salts seep through the cracks, the reinforcement becomes corroded. This ultimately leads to bridges with lower lifespans that require costly rehabilitation.

A case study was done in New Jersey by implementing 5 lbs per cubic yard of macro polypropylene fibers in the mix design for bridge decks. It improved transverse cracking frequency by reducing the number of cracks by 16.7% and reducing maximum crack width by 33.3%. However, the cracking frequency can still be improved by further implementing hybrid fibers into the mix design.

The objective of this experiment is to improve these cracking frequencies by implementing hybrid combinations of fibers into the mix design. Of the hybrid mixes done in this study, supplementing 5lbs per cubic yard of macro polypropylene fibers with 0.5 lbs per cubic yard of micro polypropylene fibers had favorable effects. The tensile strength was increased by 8.5% in comparison to macro fibers alone. In addition, free shrinkage was improved by 20.8%. Cracking frequencies were also surpassed in the AASHTO ring test: the number of cracks in the test was reduced by 14.6%, average microcrack width was reduced by 1.0% and the cracking area was reduced by 15.7%. In

conclusion, it is proven that hybrid fiber-reinforced concrete performs better than single fiber-reinforced concrete.

ACKNOWLEDGEMENTS

I would like to thank my academic advisor, Dr. Hani Nassif, for giving me this amazing opportunity to participate in a wonderful group that helps change society. He gave me all of his wisdom and guided me throughout my undergraduate and graduate degree.

I would also like to thank my co-advisor, Dr. Adi Abu-Obeidah. He was always there for me to answer any and all of the questions I had. I appreciate his guidance and advice he has given me throughout this past year.

I also must give credit to all of my colleagues and coworkers: Andrew Shehata, Jonathon Rodriguez, John El-Khouri, Dan Okechukwu, Tin Weng, Wassim Nasreddine, Albert Hajj Moussa, Alain Hajj Moussa, and Mirelle Alktaish. Through all the countless hours of batching, mixing, testing, crack mapping, and doing field work, you all helped me through it and I wouldn't be here without your efforts.

I'd also like thank my friends and family for their endless patience and support throughout this past year.

I also must thank all the sponsors would were involved in this project. With the help of Euclid Chemical, Clayton Concrete, and BASF Chemical, this project was made possible through all of their generous donations. I'd lastly like to thank the New Jersey Turnpike Authority for sponsoring this project and allowing me help them and the civil engineering industry.

Table of Contents

ABSTRACT OF THESIS……ii

AWKNOWLEDGEMENTS…… v

Table of Contents……... vi

List of Figures.……...ix

List of Tables……xii

1. Introduction…….....1

    1.1 Problem Statement……1

    1.2 Research Objectives……...2

2. Literature Review……4

    2.1 Introduction……4

    2.2 High Performance Concrete……...6

    2.3 Case Studies of Bridge Decks……..…10

    2.4 Types of Concrete Shrinkage……...13

    2.5 Fibers……17

    2.6 Restrained Shrinkage Test……...23

3. Experimental Program……...26

    3.1 Introduction……..26

    3.2 Material Properties……...28

    3.3 Mix Proportions……...31

        3.3.1 Mixing Procedure……32

3.3.2 Fresh Property Testing……33

3.3.3 Sampling and Curing……...35

3.4 Laboratory Testing…….……..39

3.4.1 Compressive Strength Testing……39

3.4.2 Splitting Tensile Strength Testing……...……41

3.4.3 Modulus of Elasticity Testing…… .42

3.4.4 Modulus of Rupture Testing……44

3.4.5 Surface Resistivity and Rapid Chloride Permeability Testing……45

3.4.6 Free Shrinkage Testing……48

3.4.7 Restrained Shrinkage Testing……..49

3.4.7.1 Modified AASHTO Restrained Shrinkage Testing……...54

4. Results……59

4.1 Introduction……..59

4.2 Fresh Properties……...60

4.3 Mechanical Properties……..62

4.3.1 Compressive Strength……..62

4.3.2 Splitting Tensile Strength……64

4.3.3 Modulus of Elasticity ……..66

4.3.4 Modulus of Rupture……68

4.4 Surface Resistivity and Rapid Chloride Permeability……70

4.5 Free Shrinkage……72

4.6 Restrained Shrinkage……...74

4.6.1 $M^0N^0S^0$……75

4.6.2 $M^0N^0S^{42}$……..…77

4.6.3 $M^5N^0S^0$……79

4.6.4 $M^{2.5}N^{0.5}S^0$……81

4.6.5 $M^5N^{0.5}S^0$……...83

4.6.6 $M^0N^{0.5}S^{12.5}$……...85

4.6.7 $M^5N^0S^5$……87

4.6.8 $M^5N^0S^7$……89

4.7 Crack Mapping Comparison……91

4.7.1 Number of Cracks……91

4.7.2 Average Crack Width……..93

4.7.3 Maximum Crack Width……...96

4.7.4 Cracking Area……..98

4.7.5 Average Crack Length……...100

4.8 Mix Ranking……..101

5. Conclusion……..….105

6. Bibliography……..……..109

List of Figures

Figure 2.1 Concrete advancements in high-rise construction (Aitcin 1998) ……..…7

Figure 2.2 Crack measuring tool (Brewer 2018) …….…….…….……...13

Figure 2.3 Experimental procedure in measuring chemical shrinkage (Tazawa et. al 1994).. …….…….…….…….…….…….……14

Figure 2.4 Influence of aggregate type on drying shrinkage (Troxell, G.E. et al. 1958) Proc. ASTM, Vol. 58, 1958; and ACI Monograph 6, 1971, pp.128, 151…..……16

Figure 2.5 Free shrinkage of concrete made with steel and polypropylene at 1% by volume (Grzybowski & Shah 1990) …….…….…….……..22

Figure 2.6 Free shrinkage of SCC reinforced with increasing amounts of micro-polypropylene fibers (Ghanchi 2015) …….…….…….……23

Figure 2.7 AASHTO standard ring dimensions …….…….…….….24

Figure 3.1 Micro, macro, and steel fibers under investigation …….……28

Figure 3.2 Sieve analysis for coarse and fine aggregates …….……30

Figure 3.3 Mixer instrumented to produce concrete …….…….……...33

Figure 3.4 Slump cone for fresh property tests …….…….…….……..34

Figure 3.5 Air meter for fresh property tests …….…….…….……34

Figure 3.6 Cylindrical, flexure, and free shrinkage molds for typical mix ……...36

Figure 3.7 AASHTO ring molds for typical mix …….…….…….……...36

Figure 3.8 Environmental chamber held at constant temperature of 74˚and 50% humidity. …….…….…….…….…….…….……37

Figure 3.9 Wet-curing of AASHTO ring specimen …….……38

Figure 3.10 Forney testing machine used to for compression, tension, and elastic modulus tests ……40

Figure 3.11 Capped cylinder in testing machine ……41

Figure 3.12 Tensile strength testing of samples with and without fibers ……42

Figure 3.13 Test sample with modulus cage in testing machine ……43

Figure 3.14 Testing set-up for rupture modulus ……44

Figure 3.15 Tested fiber-reinforced flexure samples ……45

Figure 3.16 Surface resistivity meter ……46

Figure 3.17 Rapid chloride permeability cells ……47

Figure 3.18 Free shrinkage length comparator ……49

Figure 3.19 AASHTO ring specimen with a visible full depth macrocrack……50

Figure 3.20 Standard and modified AASHTO ring specimens ……51

Figure 3.21 Dinolite software used to measure crack widths found with microscopic camera ……53

Figure 3.22 Crack width growth between 28 and 56 days ……54

Figure 3.23 Hexagonal bolt tool to allow for VWSG instrumentation ……55

Figure 3.24 Modified AASHTO ring specimen with VWSGs ……55

Figure 3.25 Example of VWSG data used to determine age of cracking (Ghanchi 2015)……56

Figure 4.1 Compressive strength vs. time ……63

Figure 4.2 Splitting tensile strength vs. time ……65

Figure 4.3 Modulus of elasticity vs. time ……67

Figure 4.4 Modulus of rupture vs. time ……69

Figure 4.5 Free shrinkage vs. time ……73

Figure 4.6 $M^0N^0S^0$ FSG Data ……...76

Figure 4.7 $M^0N^0S^0$ Ring Stress ……76

Figure 4.8 $M^0N^0S^{42}$ FSG Data ……..78

Figure 4.9 $M^0N^0S^{42}$ Ring Stress ……78

Figure 4.10 $M^5N^0S^0$ FSG Data ……80

Figure 4.11 $M^5N^0S^0$ Ring Stress ……...80

Figure 4.12 $M^{2.5}N^{0.5}S^0$ FSG Data ……..82

Figure 4.13 $M^{2.5}N^{0.5}S^0$Ring Stress ……82

Figure 4.14 $M^5N^{0.5}S^0$ FSG Data ……84

Figure 4.15 $M^5N^{0.5}S^0$Ring Stress ……..84

Figure 4.16 $M^0N^{0.5}S^{12.5}$ FSG Data ……86

Figure 4.17 $M^0N^{0.5}S^{12.5}$ Ring Stress ……..86

Figure 4.18 $M^5N^0S^5$ FSG Data ……88

Figure 4.19 $M^5N^0S^5$ Ring Stress ……...88

Figure 4.20 $M^5N^0S^7$ FSG Data ……90

Figure 4.21 $M^5N^0S^7$ Ring Stress ……...90

Figure 4.22 Number of cracks vs. time ……..92

Figure 4.23 Average crack width vs. time ……93

Figure 4.24 28-day average crack width statistical comparison……94

Figure 4.25 56-day average crack width statistical comparison……94

Figure 4.26 Maximum crack width vs. time ……..96

Figure 4.27 Cracking area vs. time ……...98

List of Tables

Table 3.1 Summary of experimental tests and days conducted ……...26

Table 3.2 Material specifics and sources ……...29

Table 3.3 Fiber properties……..…29

Table 3.4 Properties of coarse and fine aggregates ……30

Table 3.5 Mix design proportions ……31

Table 3.6 Summary of tests performed ……39

Table 4.1 Summary of mix designs with varying fiber doses ……60

Table 4.2 Summary of fresh property results ……61

Table 4.3 Compressive strength results ……63

Table 4.4 Splitting tensile strength results ……65

Table 4.5 Modulus of elasticity results ……..67

Table 4.6 Summary of modulus of rupture results ……69

Table 4.7 Summary of surface resistivity results (kOhm-cm) ……70

Table 4.8 Summary of rapid chloride permeability results (coulombs) ……..71

Table 4.9 56-day free shrinkage results ……72

Table 4.10 $M^0N^0S^0$ 28-day crack mapping results ……75

Table 4.11 $M^0N^0S^0$ 56-day crack mapping results ……75

Table 4.12 $M^0N^0S^{42}$ 28-day crack mapping results ……77

Table 4.13 $M^0N^0S^{42}$ 56-day crack mapping results ……77

Table 4.14 $M^5N^0S^0$ 28-day crack mapping results ……79

Table 4.15 $M^5N^0S^0$ 56-day crack mapping results ……79

Table 4.16 $M^{2.5}N^{0.5}S^0$ 28-day crack mapping results ……..81

Table 4.17 $M^{2.5}N^{0.5}S^{0}$ 56-day crack mapping results ……...81

Table 4.18 $M^{5}N^{0.5}S^{0}$ 28-day crack mapping results ……83

Table 4.19 $M^{5}N^{0.5}S^{0}$ 56-day crack mapping results ……83

Table 4.20 $M^{0}N^{0.5}S^{12.5}$ 28-day crack mapping results ……85

Table 4.21 $M^{0}N^{0.5}S^{12.5}$ 56-day crack mapping results ……85

Table 4.22 $M^{5}N^{0}S^{5}$ 28-day crack mapping results ……..87

Table 4.23 $M^{5}N^{0}S^{5}$ 56-day crack mapping results ……87

Table 4.24 $M^{5}N^{0}S^{7}$ 28-day crack mapping results ……89

Table 4.25 $M^{5}N^{0}S^{7}$ 56-day crack mapping results ……89

Table 4.26 Number of cracks comparison ……91

Table 4.27 Average crack width (in) comparison ……93

Table 4.28 Maximum crack width (in) comparison ……..96

Table 4.29 Cracking area (in^2) comparison ……98

Table 4.30 Average crack length comparison (in)……...100

Table 4.31 Mix ranking weight & points……102

Table 4.32 Mix ranking……103

1. Introduction

In the following section, the advantages and disadvantages of high performance concrete are briefly described. Its application in bridge slabs are very common, but one critical issue in implementing HPC in bridge decks is transverse cracking. The cause of this cracking is explored and potential solutions are investigated.

1.1 Problem Statement

Concrete is the most common structural material used in the entire world (Brewer 2018). It's cheap ingredients and ability to form into any shape makes it an extremely versatile tool that is used in structures everywhere. High-performance concrete is commonly used in bridge decks as it provides higher tensile strength and lower shrinkage than Class A concrete (Brewer 2018). But a higher tensile strength does not necessarily increase the durability of the mix. If bridge decks have many cracks, especially those that are wide, deicing salts may seep through the cracks and can potentially corrode the reinforcements. This results in reducing the service life of bridges that need their decks replaced more frequently. As a result, many DOTs are investigating solutions to this problem as it can become very expensive and critical if it is not addressed.

In slab-on-girder bridges, the concrete slab is typically held in place by a steel deck that sits on top of the girder. The top surface is exposed to undesirable conditions like high temperature gradients, deicing salts, and drying from the atmosphere. A consequence of this is that the slab is subjected to restrained conditions: the bottom surface is held in place by the deck and the top surface is free. These restrained conditions are ultimately why the concrete cracks. If the cracking frequency of the mix can be reduced and mitigated then replacement of the deck can be delayed.

Fibers can be implemented into a concrete mix to increase cracking resistance. Once the curing of concrete ceases and drying begins, the cement hydrates itself by "consuming" the water in the mix. Exposed members of concrete elements are subjected to ambient conditions that dry the moisture out of the concrete, causing the member to shrink. The various types of shrinkage will be investigated later in this paper.

Another advantage to adding fibers into concrete is to reduce crack width and crack propagation into the steel reinforcement. As previously stated, before a visible macro crack occurs in any concrete member, a large amount of small micro cracks occurs. If fibers are present, they will intercept the crack and absorb the tensile stress that occurs in the concrete. This ultimately reduces crack width and could prevent macro cracks from occurring altogether.

1.2 Research Objectives

The main objective of this research is to determine which combinations of hybrid fibers will reduce cracking frequency of high-performance concrete under restrained shrinkage conditions. The types of fibers under investigation are macro 2" polypropylene fibers, micro ¾" polypropylene fibers, and crimped 1.5" steel fibers. The types of hybrid fibers and dosages of each will be the varying parameters of this experiment. The main test used to assess cracking frequency is the AASHTO PP-34 ring test (restrained shrinkage test). This test will give incite on various cracking parameters of each mix such as average crack width, maximum crack width, crack area, etc. Other tests will also be conducted: compression, modulus of elasticity, tension, free shrinkage, modulus of rupture, surface resistivity (SR), and rapid chloride permeability. The effects on mechanical properties will be investigated. Adding fibers to the mix should show a slight

trend in reduction of shrinkage, reduction of cracks due to crack interception, and an increase in tensile strength. The negative effects of adding fibers will also be noted. One of the most major concerns is reduction in workability and the applicability of the mix. In addition, incorporating steel fibers raises concerns in regards to the natural corrosive behavior of steel when exposed to air and water. In conclusion, the primary objective of this research is to determine which combination of hybrid fibers will improve cracking resistance frequency that provides an optimal and feasible mix design for slab-on-girder bridge decks.

2. Literature Review

In the following section, the history of HPC and its evolution are described. The advantages as well as disadvantages in utilizing HPC for bridge slabs are explored. The main problem in bridge decks is transverse cracking, which results in expensive rehabilitation of the structures. The main focus of this experiment is to improve the cracking frequency of bridge decks exposed to restrained shrinkage conditions by implementing more than one type of fiber into the mix design.

2.1 Introduction

High performance concrete is commonly used in bridge slabs as its higher strength and superior durability provide a better performance than conventional mixes. What characterizes HPC is the addition of SCM's (substitute cementitious materials) combined with a low water to cement ratio. Replacing doses of cement with SCMs like fly ash, silica fume, and slag offers a variety of advantages then using cement alone (R.P Khatri et. al 1994). The low water to cement ratio is essential, so adding superplasticizers is required for any workability and constructability. All of these constituents are what allows HPC to have superior strength and permeability, making it an excellent material choice for bridge decks.

Cracking may occur in high performance concrete for a plethora of reasons. Concrete mixes with a low water to cement ratio are made possible because of the availability of superplasticizers. A low water/cement ratio may increase strength and durability, but also results in high rates of self-desiccation which may increase the potential in early age cracking (Shen et. al 2017). This is also known as autogenous shrinkage.

Another instance when transverse cracking occurs is during deck replacements. When one lane is being poured and adjacent lanes are open to traffic, some stress is transferred into the lane that has fresh concrete. In addition, vibrations are transferred to the fresh concrete, which often causes the reinforcement to not bond completely with the concrete (Abu-Obeidah et. al 2019). As a result, it was determined that concrete must have a minimum strength of 1200 psi within 6 hours of casting in order to combat this transverse cracking (Abu-Obeidah et. al 2016).

Cracking may also occur due to various types of shrinkage. The main types are chemical, autogenous, drying, thermal, and plastic shrinkage. Shrinking of concrete occurs in the short term as well as the long term. Chemical shrinkage occurs in the early stage of cement hydration, as the products of the chemical reaction naturally have less volume than the reactants (Wu et. al 2017). Autogenous shrinkage is defined as the shrinking that occurs without any volume change, moisture loss, or temperature variation (Wu et. al 2017). This is a byproduct of the cement hydration process and is inevitable. Drying shrinkage occurs due to the evaporation of water in the concrete matrix to the environment. Thermal shrinkage transpires when a temperature gradient is present which causes uneven expansion and contraction (Wu et. al 2017) amongst a concrete element. Carbonation shrinkage is caused when CO_2 in the atmosphere reacts with the calcium hydroxide present in concrete. All of the causes of volume change are extremely vital especially when concrete is under restraint. Restraint is inevitable in structures, but if one can mitigate shrinking then cracking may be minimized.

Concrete has a natural brittle tendency and is very weak in tension. Although designed to always be subjected to compression, shrinkage and creep induce tensile

stresses, sometimes high enough to cause cracking. As a result, fibers are added to the matrix to increase tensile strength and reduce shrinkage-induced cracking. The size, dose, and strength of fibers provide numerous effects and will be investigated to provide the optimal mix design in bridge decks.

2.2 High Performance Concrete

The history of HPC started with the introduction of high strength concrete (HSC). P.C. Aitcin's book, High Performance Concrete, illustrates the history and evolution of HPC. It states that high strength concrete started in the 1960s in the city of Chicago. Designers were interested and eager to discover that concrete can be produced with a compressive strength up to 60 MPa (8700 psi) rather than 20 MPa (2900 psi). The increase in floor spacing and smaller column sizes was now possible, something designers, contractors, and owners could benefit from. What made HSC possible was the transition from water reducers to superplasticizers. Superplasticizers were first originally used on site right before pouring (Aitcin 2004). They acted as a fluidifier to prevent segregation and reduction of strength when extra water was added. As manufacturing advanced, high doses of superplasticizer could be added to concrete without retarding the cement hydration process or entrapping too much air. Although advancements were done on increasing the compressive strength of concrete, durability was still not improved.

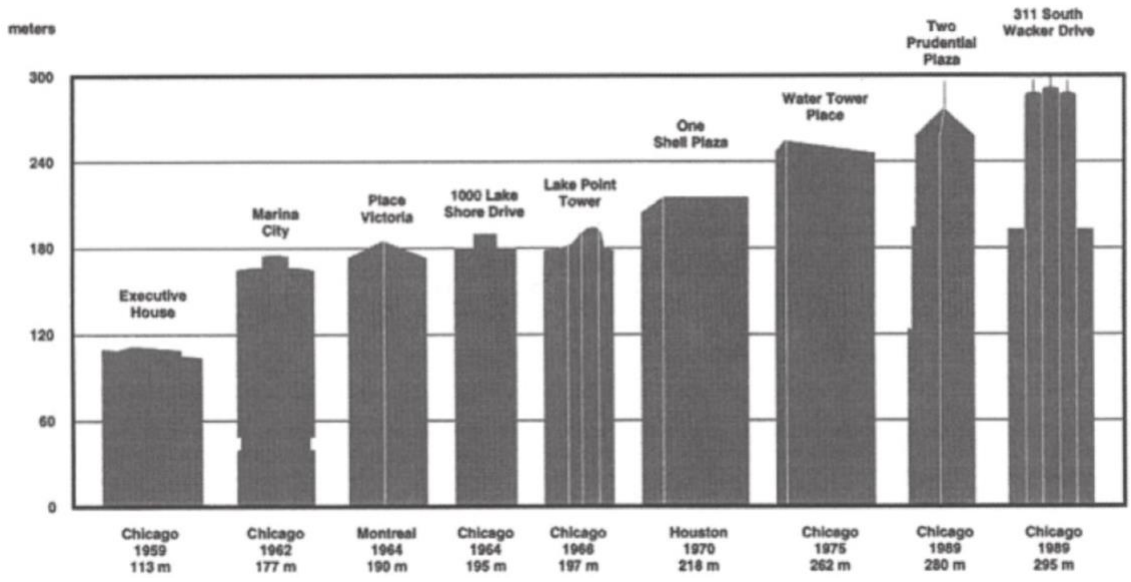

Figure 2.1 – Concrete advancements in high-rise construction (Aitcin 1998)

Another chemical admixture that is added to concrete to increase its durability is air entraining admixtures (AEA). Their role is to supply hydrated concrete with micro-pockets of air. This is done to prevent internal cracking that occurs from repeated cycles of freezing and thawing. "Such an air void system is also necessary in most cases to produce deicer salt scaling-resistance concrete" (Pigeon et. al 1995). This is absolutely crucial especially in colder climates. To ensure a necessary amount of air pockets, an air test is performed for fresh concrete, similar to the slump test. If concrete mixes have low air contents, the trucks may be rejected. In addition, too many air pockets results in concrete with lower compressive strength. The desired range is typically 3%-7.5% in fresh concrete based on the maximum aggregate size (Kosmatka 1998). Adding air entraining admixtures to HPC is crucial for long term durability of concrete members.

Pierre-Claude Aitcin's book, High Performance Concrete, advises that silica fume began being used as a SCM in Scandinavia in the 1970s. In his book, he illustrates the history and discovery of using silica fume as a SCM. Silica fume is a byproduct of the

silicon and ferrosilicon manufacturing process (Aitcin 2004). For years, it was released into the environment as a pollutant because its potential was not yet discovered. After strong regulation from the government, companies began collecting this fine dust and attempted to find ways to use it. Due to the diligent research efforts conducted in the 1980s, the positive effects of adding silica fume to concrete became widespread and its implementation in manufacturing began all over the world (Aitcin 2004). Silica fume is required in production of HPC and is considered a key element in the matrix of this durable material.

Using silica fume as a SCM is a necessity for the fabrication of HPC. Firstly, the fine particle size results in a reduction of workability, therefore requiring higher doses of superplasticizer in order to maintain slump (R.P Khatri et. al 1994). Khatri also reported that adding silica fume to Portland cement increases strength at all ages. In addition, he proclaimed that silica fume increases short-term drying shrinkage when prepared with Portland cement, but decreases long term shrinkage in comparison to concrete prepared with cement alone. In conclusion, adding silica fume provides clear benefits if higher doses of superplasticizers are available.

Other effects on mechanical properties also occur when using silica fume as a SCM. It was reported that using silica fume tends to reduce the rate of increase of the elastic modulus with age (Nassif et. al 2005). According to Nassif, this is due to a high rate of hydration when silica fume is implemented. A result of this fast hydration is a high modulus of elasticity at an early age (Nassif et. al 2005). This may be preferred when decks are poured overnight and opened to traffic within a short period of time.

Fly ash is also used as a supplementary cementitious material in producing HPC. Its production is a byproduct of coal-fired power plants (Mehta 2004). Incorporating fly ash into a concrete mix has numerous advantages. First and foremost, it acts a water reducer, primarily reducing the water required for a specific consistency (Mehta 2004). As a result of this, the total paste content of the mix may be reduced, therefore reducing drying shrinkage (Mehta 2004). In addition, Mehta also claims that microcracks have a major role in permeability and durability of concrete exposed to severe environmental conditions. The pozzolanic reaction that comes with adding fly ash reduces the size of capillary pores that occur with cement hydration (Mehta 2004). This reduction in size reduces the overall thickness of the pores and increases the strength of the microstructure. Consequently, concrete mixes supplemented with fly ash have higher durability against cracking and provide better permeability when exposed to harsh environments (Mehta 2004). It is clear that incorporating fly ash into an HPC mix design has its clear advantages in making concrete more durable.

Another supplementary cementitious material often used in HPC is blast furnace slag. A benefit from using slag is its ability to reduce CO_2 emissions that is associated with the production of cement (Samad & Shah 2017). Because cement requires large amounts of heat and power to be manufactured, replacing quantities of cement with slag reduces the carbon footprint of concrete production. What makes this possible is that large quantities of cement can be replaced with slag. Samad and Shah hypothesize that utilizing slag also increases compressive and flexural strength in comparison to concrete only made with cement. In addition, they discovered that to receive the full benefits that come from adding slag, the mix design must have a maximum 50% replacement with

cement. Due to its ability to compact, it also increases workability and lowers air content (Samad & Shah 2017). It is evident that replacement of cement with blast furnace slag can be beneficiary, but it must be instrumented correctly.

2.3 Case Studies of Bridge Decks

A critical infrastructure issue that is recognized by many DOTs across the country is transverse cracking of concrete for slab-on-girder bridges. It is known that many transverse cracks occur very soon after the bridge deck is constructed. This can cause a number of legal issues between DOTs and contractors. Cracking occurs due to a combination of concrete properties and restraint from the girders. Many studies have been conducted to elongate bridge life by mitigating cracking in the slab. Progress has been made in this effort to reduce cracking, yet it is still a costly issue that continues to reduce the life of bridges everywhere.

Cracking occurs in bridge decks for a plethora of reasons. The critical parameters regarding transverse cracking include end restraint, girder stiffness, cross frame location, splice location, deck rebar cutoff length, concrete shrinkage characteristics, concrete elastic modulus, and temperature (French et. al 1999). Some of these parameters can be addressed with fibers and proper staged construction. Due to the research conducted over the past few decades, standards were implemented in design codes to improve bridge life. Some of which are utilization of epoxy-coated reinforcement, minimum cover of 3”, and a minimum deck thickness of 9” (French et. al 1999).

Catherine French performed a case study of bridges in Minnesota. The study concluded that simply-supported prestressed girder bridges provide better performance in terms of transverse cracking of bridge decks in comparison to continuous steel girder

bridges (French et. al 1999). This was due to the reduced end restraint and lower creep parameters of the prestressed girders. In addition, the size of the top transverse reinforcement in steel girder bridges has an influence on cracking behavior (French et. al 1999). The bridges that performed the best had No. 5 bars at 5.5" spacing or No. 6 bars at 6.5-7" spacing (French et. al 1999). French also concluded that continuous multi-span bridges with stiff girders and thin decks experienced severe transverse cracking. She reported that most cracks occur at railing parapet joints and cross frame locations. To expand, she similarly states that bridges with expansion joints experience less cracking than similar bridges without expansion joints. This can be attributed to less restraint during thermal expansion.

Progress has also been conducted to improve the mix design for bridge decks. The critical parameters of the mix design are cement content, aggregate type and quantity, and air content (French et. al 1999). Mixes with high cement content (847 lb/yd^3) cracked much earlier than mixes with considerably less cement (470lb/cy^3) (French et al 1999). Generally, it is recommended to reduce paste content to mitigate shrinkage. In addition, the mix with a high amount of coarse aggregate (1845 lb/yd^3) and high amount of fine aggregate (1203 lb/yd^3) exhibited the least amount of cracking (French et. al 1999). This can be attributed to the reduction of paste content per cubic yard.

In addition, some practices can be performed in the field to reduce cracking of bridge decks. The optimal ambient temperatures to cast a bridge slab is a low of 45 to 50˚ and a high of 65-70˚ (French et. al 1999). In warm weather, casting at night tended to reduce thermal shrinkage and reduce future cracking (French et. al 1999). Deck pours in extreme hot and cold temperatures similarly performed poorly and cracked severely

(French et. al 1999). In addition, staged deck construction also plays a role in transverse cracking. When replacing a bridge deck, lanes that are adjacent and open for traffic have a high potential to induce tensile stresses in fresh concrete, which can lead to premature cracking. Lap splices of transverse rebar resulted in cracking in one half of the longitudinal direction, implying that splicing may increase the degree of restraint (French et. al 1999). It is vital to investigate and enforce optimal construction practices in order to prevent early age cracking of concrete bridge decks.

Utilization of fibers for concrete bridge slabs is relatively new and further case studies must be conducted. Of the few that were done, Gregory Brewer's case study of FR-HPC exhibits positive effects in transverse cracking of bridge decks (Brewer 2018). The study aimed to investigate and quantify the cracking frequency of actual slabs casted with FR-HPC. There were two mixes casted: one control HPC mix and an identical mix with 5 lb/yd^3 of 2" polypropylene macrofibers added. The 8 – 200' slabs were crack mapped with a crack card as shown in Figure 2.2. The data collected included maximum crack width and spacing of cracks. To reduce bias, the data was collected by Brewer and an outside contractor. The FR-HPC reduced the number of cracks by 16.7% observed by Brewer, while the outside contractor observed a reduction of 13.7%. In the positive moment region, average crack widths were reduced by 16.7% and maximum crack widths were reduced by 33.3%. In the negative moment region, average crack widths were reduced by 18.1% while maximum crack widths were not affected. Cracking area was also reduced by 33.4%. There is undeniably a reduction of cracking frequency when polyprolyene fibers are added to the mix design. Improvements can still be made to the fiber mix design in order to reduce this frequency even further.

Figure 2.2 – Crack measuring tool (Brewer 2018)

2.4 Types of Shrinkage

In order to reduce shrinkage of concrete, the various types of shrinkage must be investigated. The first type of shrinkage to occur in fresh concrete is chemical shrinkage. The basis of this type of shrinkage is that the volume of hydrated cement is less than the total volume of unhydrated cement and water. This is also called hardening shrinkage (Tazawa et. al 1994). Tazawa suggests a method for quantifying the amount of chemical shrinkage that occurs for cement paste as shown in Figure 2.3. He also hypothesizes that if one can predict the amount of chemical shrinkage at 100% hydration, then it is possible to predict the degree of hydration at any age. Chemical shrinkage is inevitable and should not be the main focus of reducing concrete volume changes.

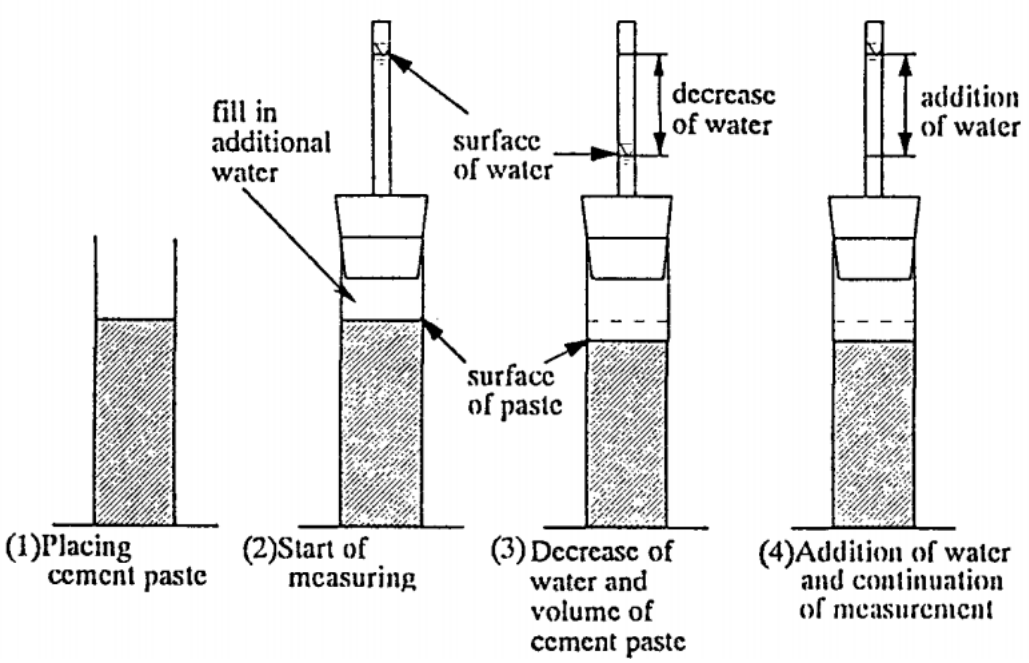

Figure 2.3 – Experimental procedure in measuring chemical shrinkage (Tazawa et. al 1994)

Autogenous shrinkage is a critical type of shrinkage, specifically in mixes with low water/cement ratios. The Japanese Concrete Institute defines autogenous shrinkage as "the macroscopic volume reduction of cementitious materials when cement hydrates after initial setting" (Jiang et. al 2014). Autogenous shrinkage does not include volume change due to loss or ingress of substances, temperature variation, and application of an external force and restraint" (Burrows 1998). This is sometimes referred to as self-desiccation. As curing progresses, the cement hydrates itself with water found in the capillary pores of concrete (Tazawa 1999). When this occurs, the surface tension between the pores and the water causes the pore walls to close, causing the volume of concrete to decrease. Because of HPC's low water/cement ratio, reducing autogenous shrinkage can dramatically increase cracking resistance against restrained conditions.

Recent research has discovered multiple ways to combat autogenous shrinkage. Firstly, wet-curing methods provide an external source of hydration for concrete elements. In addition, it has been recently discovered that substituting some of the fine aggregate with lightweight aggregate (LWA) has the potential to reduce rates of autogenous shrinkage (Bentz & Weiss 2011). LWA has similar characteristics to sand, yet the main difference is its very high rate of water adsorption. When the concrete cures, the cement absorbs some of the water reservoirs that is stored in the LWA (Bentz & Weiss 2011). This is often referred to as internal curing. According to Weiss and Bentz, actual bridge decks casted with LWA reported no visual cracking 40 days after casting. This method provides ways to combat shrinkage cracking without any extreme modifications to the mix design.

Long term volume reduction of concrete is caused by drying shrinkage. Saturated cement paste is not volumetrically stable when exposed to ambient humidity that is below saturation (Mehta & Monteiro 2006). This is due to the evaporation of adsorbed water from hydrated cement paste. Similar to autogenous shrinkage, the water stored in the capillary pores are brought to the surface due to ambient humidity and eventually evaporated into the atmosphere. When this occurs under restrained conditions, tensile stresses are induced.

One important parameter that plays a major role in drying shrinkage is the modulus of elasticity of the aggregate (Mehta & Monteiro 2006). Mehta and Monteiro state that both drying shrinkage and creep increased 2.5 times when a low elastic modulus aggregate was substituted with a high elastic modulus aggregate. As shown in Figure 2.4, aggregate with a high elastic modulus display lower rates of drying shrinkage.

Therefore, aggregate sourced from limestone or quartz are favorable in terms of reducing drying shrinkage.

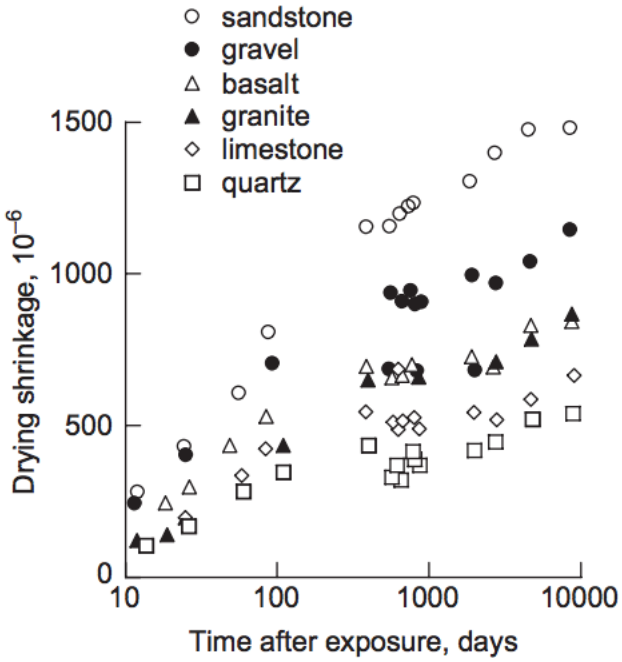

Figure 2.4 – Influence of aggregate type on drying shrinkage (Troxell, G.E. et al. 1958) Proc. ASTM, Vol. 58, 1958; and ACI Monograph 6, 1971, pp.128, 151

Another long-term cause of volume change of concrete is carbonation shrinkage. Carbon dioxide (CO_2) from the atmosphere reacts with calcium hydroxide ($Ca(OH)_2$) present in concrete producing calcium carbonate ($CaCO_3$) and water (Jerga 2004). Jerga furthermore informs that this carbonation results in a decrease of pH value and corrosion of steel reinforcement. He also recorded that shrinkage due to carbonation was increased up to 0.35%. It is evident that carbonation has a detrimental effect on concrete's durability.

The cement hydration process is an exothermal process, and the heat associated with the chemical reaction has potential to cause shrinkage cracks. It is important to control the release of this heat, especially in large structures where the presence of heat is

exponentially greater. According to Mehta and Monteiro, thermal shrinkage cracks occur not when the member is heated up, but rather when it is exposed to ambient conditions. If a concrete member is free to move under thermal shrinkage, then no stress is induced in the member. Typically, there is always some restraint present due to a steel deck or column, and as a result, shrinkage cracks may occur. Fortunately for steel bridge decks, the slabs are thin and thermal shrinkage is not a primary concern for the reason of cracking in non-high early strength mixes.

2.5 Fibers

The primary purpose of adding fibers into concrete is to reduce and mitigate cracking of concrete. As microcracks propagate into macrocracks, fibers intercept the cracks as they grow and absorb the tensile stress. It is assumed that fibers also reduce shrinkage by adding resistance to volume change. The main parameters involved in fiber-reinforced concrete (FR-C) are material type, fiber geometry, fiber distribution, fiber orientation, and fiber concentration (Zollo 1997).

Zollo claims that all types of fibers, when implemented in the correct dosages, improve fracture toughness in immature and mature concrete specimens (Zollo 1997). It is also reported that adding fibers provides a minor improvement in compressive strength (Wafa 1990). In addition, Wafa states that modulus of elasticity increases with an increase of fiber concentration. He also concluded that flexural strength, toughness, and splitting tensile strength all improved with the addition fibers. It is important to fully understand the effects of FR-C to predict effects of hybrid fiber-reinforced concrete.

A major concern with implementing fibers into concrete is its negative impact on workability. Concrete with high slump is easier to cast and is associated with reduced

labor and cheaper costs. As a result, owners are skeptical in utilizing FR-C because of its negative effect on workability. Due to advancements in manufacturing of water-reducers, typical dosages of superplasticizers have a high range and can be used to combat this decrease in workability. Therefore, it is important to find the right concentration of fibers to implement in order to prevent concrete from being unworkable.

In addition, whether fibers have any effect on the percentage of entrapped air in fresh concrete is critical. A study concluded that, in general, implementing fibers reduces fresh air content (Balaguru & Ramakrishnan 1988). Another study reported that air content decreases with increasing fiber content (Eren & Çelik 1997). They predicted that this may be a result of the fibers allowing for a network of air bubbles to escape. In conclusion, the reduction of entrapped air should be monitored when implementing fibers in concrete.

Another undesired effect of adding fibers into a concrete mix is an increase in permeability. Due to fibers taking up space in the matrix, a chloride solution will be able to penetrate through concrete more easily. It was reported that incorporating polypropylene fibers into a concrete mix increases permeability, but this increase may be reduced with the addition of silica fume (Toutanji 1998).

Steel fibers are often chosen in FR-C for a plethora of reasons. Steel is much more ductile and has a higher failure stress than concrete. Its implementation in a concrete mix has great potential in increasing concrete's mechanical properties. A report about steel fiber-reinforced concrete concluded that high-strength steel fiber-reinforced concrete exhibits a 19.3% improvement in splitting tensile strength and a 28.1% increase in modulus of rupture (Song & Hwang 2004). In addition, a study was done by Calogero

Cucchiara on steel-fiber reinforced concrete beams to determine their influence in shear failures. It was determined that the addition of steel fibers caused the beams to display a more progressive crack pattern rather than a sudden one with smaller crack widths (Cucchiara 2004). It was also concluded that the inclusion of steel fibers transformed a brittle shear failure into a more ductile flexural failure. Cucchiara further states that implementing steel fibers allows for more energy dissipation which may be beneficial for concrete members subjected to extreme events (Cucchiara 2004). It is evident that the mechanical properties of concrete are improved significantly when steel fibers are added to the matrix.

A major disadvantage of utilizing steel fibers in concrete is their natural tendency to corrode. Although the mechanical properties can be improved greatly, the durability of concrete reinforced with steel fibers requires significant investigation. Corrosion comes into play once the concrete member cracks, as chlorides may seep into the crack and corrode not only reinforcement, but the steel fibers themselves. A study was done and it was determined that cracks less than 0.20 mm wide provides resistance against corrosion and the element is unaffected by corrosion of the fibers (Marcos-Meson 20018). The same study reassures that the effects of fibers experiencing corrosion is still unclear, and the focus should be on the residual strength of concrete elements with corrosion of steel fibers. If steel fibers are chosen to be the fiber implemented in FR-C, it is important to evaluate the risks involved with steel fiber-reinforced concrete.

Another fiber commonly used to reinforce concrete is synthetic polypropylene fibers. Concrete reinforced with polypropylene fibers at a concentration of 0.3% by volume displayed an increase in flexural toughness by 387% (Alhozaimy et. al 1996). In

addition, the same study concluded that the presence of polypropylene fibers increases the first crack failure and failure impact resistance of concrete. Another study investigated the mechanical properties of concrete reinforced with macro synthetic polypropylene fibers. A 15.49% increase in tensile strength was shown in comparison to concrete without any fibers (Hasan et. al 2011). Hasan also claims that polypropylene fibers provide an increase of 65.10% in shear strength. Synthetic polypropylene fibers are a common choice for FR-C and there is undeniable evidence proving their benefits.

A common parameter to consider when selecting fibers is the size of fiber. Macrofibers are typically long and thick such that they provide flexural strength and toughness when added to concrete. In addition, they are visible and have a distributed orientation in the matrix. Microfibers are usually thin and are added to concrete to reduce shrinkage. Due to their thin geometry, they sometimes are invisible and are well distributed to cover the entire element. According to Passuello et. al, macrofibers reduce crack width by 70%, while microfibers reduce crack width by 90% in the AASHTO ring test. The nature of macrofibers can reduce the frequency of macrocracks, whereas microfibers have potential to reduce the frequency of microcracks. Because each type of fiber and size provide various benefits, it is vital to examine the combination of hybrid fibers to determine the optimal fiber mix.

Hybrid fibers are composites of two or more types of fibers. A study was done comparing polypropylene macrofibers and polypropylene microfibers. A hybrid combination of the two fibers provide superior benefits to the mechanical properties in comparison to mixes with only one type of fiber (Hsie et. al 2008). The splitting tensile strength of the hybrid combination is 4.5% greater than the mix with only macrofibers.

(Hsie et. al 2008). In addition, the modulus of rupture of the hybrid mix is 9.2% greater than the mix with only macrofibers. There is a clear benefit in mechanical properties in incorporating macro and microfibers into a concrete mix.

It is also critical to investigate the mechanical properties of the fiber itself in order to predict its effects in concrete. The properties in question are modulus of elasticity, tensile strength, and ductility. In comparison to regular concrete, steel fibers have a high modulus of elasticity and tensile strength, while polypropylene fibers have low modulus of elasticity and tensile strength but have high elongation (Yao et. al 2003). In addition, carbon fibers have similar modulus of elasticity and tensile strength to steel fibers but cannot elongate significantly (Yao et. al 2003). A study was done to determine which combination of fibers provides the best results for mechanical properties. It was determined that a hybrid combination of steel and carbon fibers provided the greatest strength and flexural toughness because of their similar modulus and synergistic reaction between the two fibers (Yao et. al 2003). Another study done by Banthia in 2004 suggests that mixes with steel macrofibers and polypropylene microfibers provide some synergy. Synergy is referred to as a positive interaction between two or more types of fibers (Banthia 2004). Furthermore, Banthia proposes that a hybrid containing crimped polyprolyene macrofibers and polyproplyene micro fibers provides maximum synergy between the two. It is important to consider the interaction between the fibers in a hybrid mix, as their interaction will ultimately narrate its performance.

In addition to reducing crack width and increasing tensile strength, the effects fibers have on shrinkage are of upmost importance when assessing restrained shrinkage cracking behavior. A study was done an assessing the early age behavior of free

shrinkage on concrete reinforced with polypropylene fibers. It was reported that free shrinkage was reduced by 34% at an age of 24 hours (Wongtanakitcharoen & Naaman 2006).

Another study reported that adding fibers shows a slight reduction of long term drying shrinkage as shown in Figure 2.4 (Grzybowski & Shah 1990). The fibers investigated were steel and polypropylene fibers at 1% dosage by volume. From Figure 2.5, it can be concluded that steel fibers provide a slightly higher reduction in terms of free shrinkage, yet this reduction is very minor.

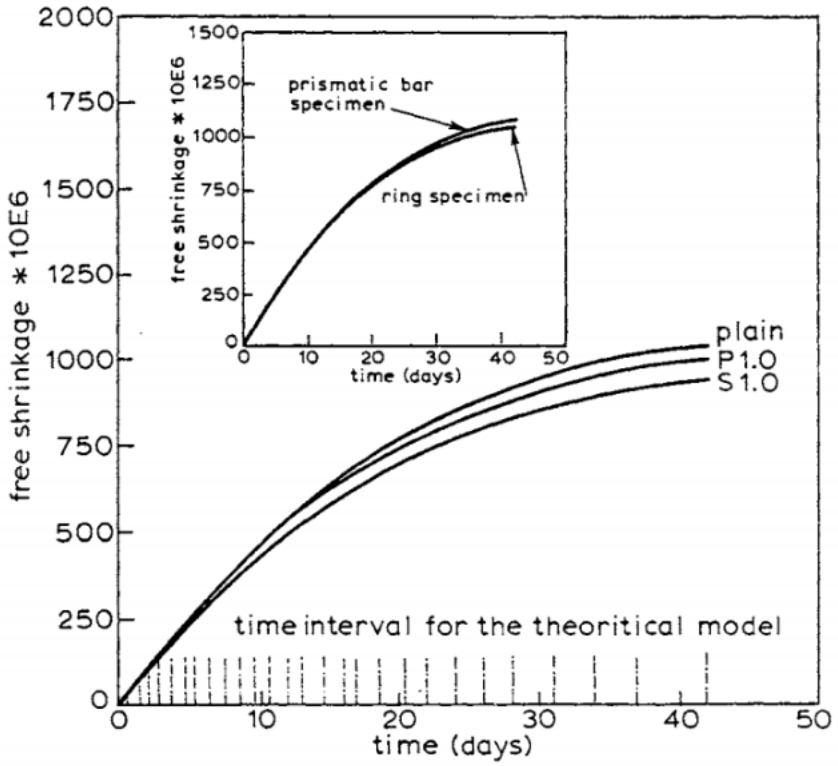

Figure 2.5 Free shrinkage of concrete made with steel and polypropylene at 1% by volume (Grzybowski & Shah 1990)

Another study was done to investigate the effects micro-polypropylene fibers have on self-consolidating concrete. It was reported that these fibers, when implemented

at 0.2% by volume, reduced free shrinkage by 9% as shown in Figure 2.6 (Ghanchi 2015). This suggests that micro-sized fibers may have a positive effect on reducing free shrinkage. In conclusion, based off of several experiments, it can be seen that adding fibers into concrete provides a great reduction of shrinkage in the early age, yet shows a very slight reduction in shrinkage in the long-term.

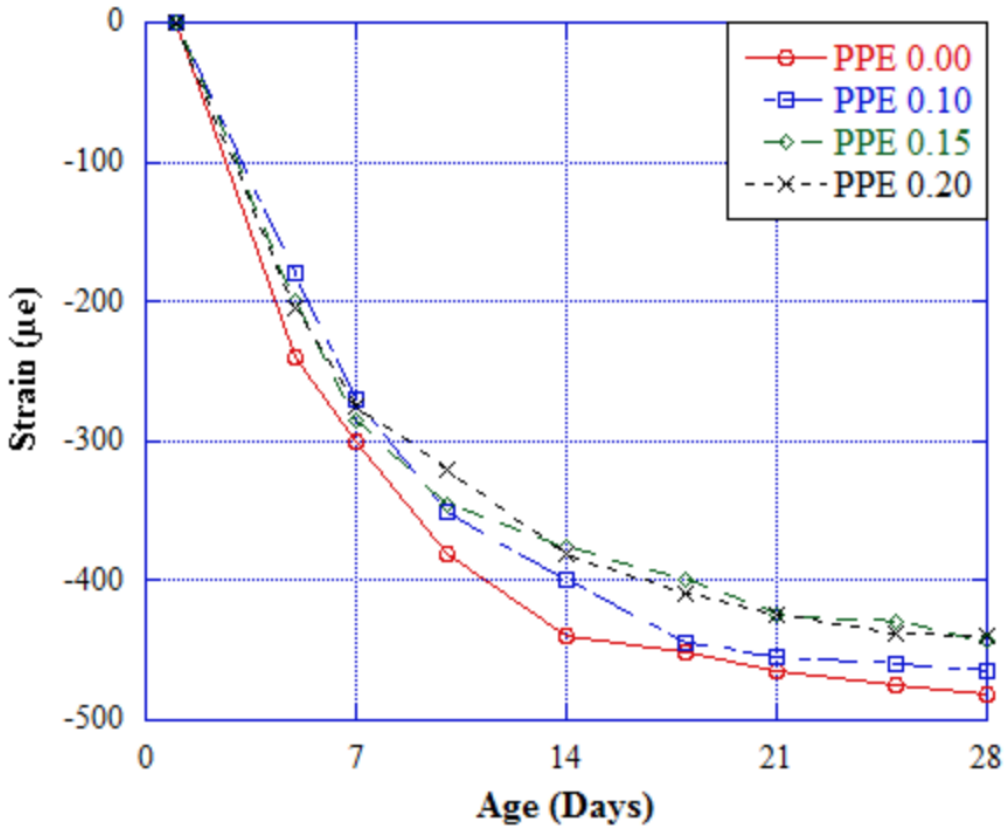

Figure 2.6 Free shrinkage of SCC reinforced with increasing amounts of micro-polypropylene fibers (Ghanchi 2015)

2.6 Restrained Shrinkage Test

In order to determine the cracking frequency of a concrete mix, a standard was developed by the American Association of Highway and Transportation Officials (AAASHTO PP-34). The test is used as a comparative tool to determine cracking

behavior of various concrete mixes. It involves concrete casted around a steel ring as shown in Figure 2.7. Because the test is used as a comparative tool, it does not quantify the behavior of actual concrete elements subjected to restrained shrinkage.

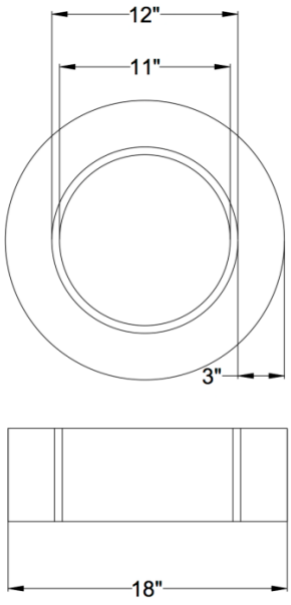

Figure 2.7 – AASHTO standard ring dimensions

As the concrete shrinks, tensile hoop stresses are induced in the concrete due to the restraint from the inner steel ring. Hossain and Weiss developed equations to determine the residual stresses present in the concrete at a given time t:

$$\sigma = -\varepsilon_{steel}(t) * E_s * C_1 * C_2 \quad (2.1)$$

ε_{steel} (t) is the strain measured in the steel ring

E_s is the elastic modulus of the steel ring

$$C_1 = \frac{R_{OS}^2 + R_{OC}^2}{R_{OC}^2 - R_{OS}^2}$$

$$C_2 = \frac{R_{OS}^2 - R_{IS}^2}{2R_{OS}^2}$$

R_{OS} is the outer radius of the steel ring

R_{OC} is the outer radius of the concrete ring

R_{IS} is the inner radius of the steel ring

By implementing the dimensions described in the AASHTO standard and using 29,000 ksi for the elastic modulus, the equation can be simplified to:

$$\sigma = -\varepsilon_{steel}(t) * 6{,}021{,}527.8 \quad (2.2)$$

This equation provides a quantifiable measure of the stress that is being developed in the concrete. It will be used later in this paper to compare with the actual stresses that are measured in the concrete ring.

3. Experimental Program

The following section illustrates the experimental program of this study. Each test and their standards are discussed in full detail.

3.1 Introduction

The experimental program of this research is aimed to identify the various effects of hybrid fiber-reinforced concrete (HFR-HPC). All of the mixes in question are cast using the same procedure and are monitored in an identical fashion. The samples are also mixed and casted according to ASTM standards. The following tests are done:

Test	Ages Conducted
Compressive Strength	1, 3, 7, 14, 28, 56 days
Splitting Tensile Strength	1, 3, 7, 14, 28, 56 days
Modulus of Elasticity	1, 3, 7, 14, 28, 56 days
Modulus of Rupture	1, 28 days
Free Shrinkage	1, 7, 14-21, 28, 35, 42, 56 days
Restrained Shrinkage	28, 56 days
Surface Resistivity	7, 14, 28, 56 days
Rapid Chloride Permeability	28, 56 days

Table 3.1 Summary of experimental tests and days conducted

All samples are demolded 23 ± 1 hours after casting is finished. 30 cylinders are casted to determine mechanical properties such as compression, tension, and modulus of elasticity. An additional 5 cylinders are casted for surface resistivity and rapid chloride permeability tests. Three free shrinkage prisms are produced to determine shrinkage after 14 days of curing. Four additional prisms are casted to determine modulus of rupture at

ages of 24 hours and 28 days. Two rings made according to AASHTO PP-34 standards and monitored for cracking properties. The only distinction from the AASHTO PP-34 standard is the curing period. Rather than drying after just one 1 day, the rings are cured for a period of 14 to mimic the curing age experienced by actual bridge decks in most bridges in New Jersey. All other samples are wet cured in 100% humidity for a period of 14 days, except rapid chloride permeability and surface resistivity samples which are wet cured for the entirety of the testing period.

All fibers examined are manufactured by Euclid Chemical Co. The fibers utilized in this study consist of 2" macro polypropylene synthetic fibers (M), ¾" micro polypropylene synthetic fibers (N), and 1.5" steel crimped fibers (S). All fibers comply with ASTM C1116. The hybrid mixes include combinations of macro & micro fibers, macro & steel fibers, and steel & micro fibers. These mixes will be compared to mixes with just one type of fiber and a control mix with no fibers. This way, individual properties of just one type of fiber can be determined and used to support hybrid fiber properties.

The doses of the fibers implemented in this experiment come from previous lab work and manufacturer recommendations. Based on previous studies, 5 lbs per cubic yard of macro fibers was deemed to be the best dose for this type of fiber. Euclid suggests implementing micro fibers at a dose of 1.0 lb per cubic yard, so hybrid combinations will consist of 0.5 lbs per cubic yard. In addition, the volume of steel fibers is to be kept consistent with the macro fibers, which is why 42 lbs per cubic yard of steel fibers are implemented as the control dose.

Figure 3.1 Micro, macro, and steel fibers under investigation

3.2 Material Properties

Material properties are investigated prior to testing to allow for more accurate and consistent data. All materials must be readily available and cost efficient so implementation in the field can be easily done. Coarse aggregates, fine aggregates, Portland cement, and silica fume are acquired from Clayton Concrete located in Edison, NJ, Clayton concrete is one of the top concrete plants in the area. A summary of the material used for the mix are summarized in the table below.

Material	Specifications	Source
Fine Aggregate	Concrete sand	Clayton Concrete
Coarse Aggregate	#57 & #8 crushed stone (3/4" & 3/8" rock)	Clayton Concrete
Portland Cement	Type 1	Clayton Concrete
Silica Fume	Densified	Clayton Concrete
Fly Ash	N/A	LaFarge North America
Macro Fibers	2" polypropylene fibers	Euclid Chemical
Micro Fibers	¾" polypropylene fibers	Euclid Chemical
Steel Fibers	1.5" crimped fibers	Euclid Chemical
Air Entraining Admixture (AEA)	MasterAir AE100	BASF Chemical
High Range Water Reducer (HRWR)	MasterGlenium 7620	BASF Chemical

Table 3.2 Material specifics and sources

Fiber Designation	Material	Length (in)	Aspect Ratio	Tensile Strength (ksi)
M	Macro polypropylene	2"	74	87
N	Micro virgin monofilament polypropylene	¾"	N/A	N/A
S	Low carbon cold drawn steel wire	1.5"	45	140

Table 3.3 – Fiber properties

The aggregates comply with standards and are tested to ensure proper gradation to ensure accurate results. The coarse aggregates are tested using sieve analysis to determine their properties according to ASTM C316. Moisture content of the aggregate is determined before each mix to ensure the correct water to binder ratio. Adsorption of the coarse and fine aggregates are determined using ASTM C127 and ASTM C128. The

aggregates are kept sealed to prevent moisture loss and dust accumulation on the top surface. The sieve analysis and aggregate properties can be seen below.

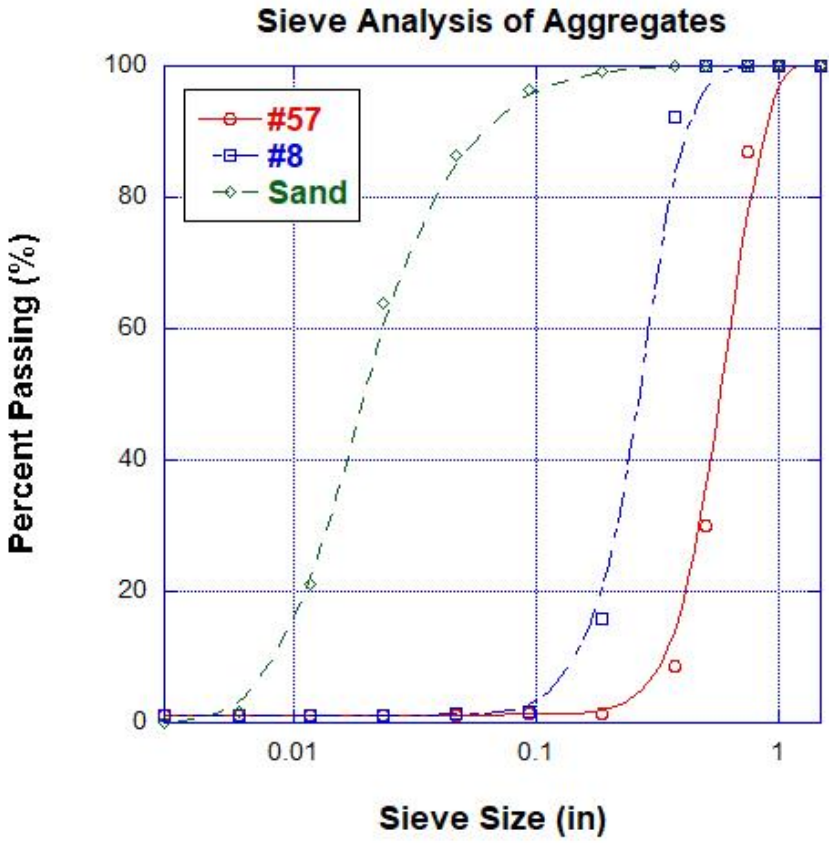

Figure 3.2 – Sieve analysis for coarse and fine aggregates

	Fine Aggregate	Coarse Aggregate
Specific Gravity	2.618	2.827
Fineness Modulus	2.347	6.026
Adsorption	0.4%	1.1%

Table 3.4 – Properties of coarse and fine aggregates

Storage of the cementitious materials are kept sealed to prevent moisture and to keep the materials dry. Cement bags are kept dry, fly ash is stored in a barrel, and silica fume is kept bagged near the cement. The Portland cement used in this study complies

with ASTM C150. Fly ash complies with ASTM C618-17a. The silica fume used complies with ASTM C1240-15.

3.3 Mix Proportions

Eight mixes were cast for this study. Of these eight, there are 5 hybrid mixes, 2 mixes with one type of fiber, and one control mix without any fibers. All of the mix proportions were kept constant, with the type and dosage of fiber being the varying parameter. Each mix had a constant volume of 4.48 ft^3.

Mix ID	**$M^0N^0S^0$**	**$M^0N^0S^{42}$**	**$M^5N^0S^0$**	**$M^{2.5}N^{0.5}S^0$**	**$M^5N^{0.5}S^0$**	**$M^0N^{0.5}S^{12.5}$**	**$M^5N^0S^5$**	**$M^5N^0S^7$**
Cement	520	520	520	520	520	520	520	520
Fly Ash	130	130	130	130	130	130	130	130
Silica Fume	25	25	25	25	25	25	25	25
Sand	1113	1113	1113	1113	1113	1113	1113	1113
3/8	300	300	300	300	300	300	300	300
3/4	1500	1500	1500	1500	1500	1500	1500	1500
Water	258	258	258	258	258	258	258	258
w/b ratio	0.382	0.382	0.382	0.382	0.382	0.382	0.382	0.382
Macro Fibers (lb/cy) (% vol.)	-	-	***5 (0.32%)***	***2.5 (0.16%)***	***5 (0.32%)***	-	***5 (0.32%)***	***5 (0.32%)***
Micro Fibers (lb/cy) (% vol.)	-	-	-	***0.5 (0.03%)***	***0.5 (0.03%)***	***0.5 (0.03%)***	-	
Steel Fibers (lb/cy) (% vol.)	-	***42 (0.32%)***	-	-	-	***12.5 (0.1%)***	***5 (0.04%)***	***7 (0.05%)***
Total Fiber (% vol.)	***0%***	***0.32%***	***0.32%***	***0.19%***	***0.35%***	***0.13%***	***0.36%***	***0.37%***
AEA (oz/cwt)	0.125	0.125	0.125	0.125	0.125	0.125	0.125	0.125
HRWR (oz/cwt)	4.4	4	5.3	5.3	4.9	4.9	4.9	4.9

Table 3.5 – Mix design proportions

3.3.1 Mixing Procedure

All of the mixes conducted in this study are done according to ASTM C192. Prior to mixing, the mixer is wet with a hose as to compensate for remaining moisture left in the mixer after casting. Also, the AEA is poured inside the batched water prior to mixing. Once the water is drained from the mixer, all of the coarse aggregate is added into the mixer with about 1/3 of the batched water. The mixer is turned on for 2-3 minutes to equally distribute the moisture amongst the coarse aggregate. Then, half of the sand is added into the mixer along with half of the cementious materials. The mixer is turned on while another 1/3 of the water is poured inside. After 2-3 minutes, the mixer is paused and inspected to ensure equal distribution of ingredients. If clumps are visible, a hoe is used to break the clumps. At this point, the rest of the sand and cementious materials are added to the mixer with the remainder of the water. Mixing occurs for another 2 minutes. Once the fresh concrete is deemed ready, the HRWR is added to the matrix and mixed for 5 seconds for equal distribution. The concrete is left for 2 minutes to allow for the chemical reaction between the cement paste and the superplasticizer to occur. Then, as the mixer is turned on, the fibers are added slowly into the matrix to prevent clumping. Mixing occurs for another 3 minutes. At this point, the mixer is turned off and testing for fresh properties begins.

Figure 3.3 – Mixer instrumented to produce concrete

3.3.2 Fresh Property Testing

The fresh properties investigated in this study are slump and air content. Slump testing is done in compliance to ASTM C143. First, the slump cone and board are moistened with water. Next, concrete is poured into the cone by thirds of the total volume. The cone is then rodded 25 times evenly, making sure the rod penetrates the previous layer by 1 inch. This process is repeated two more times. Once the cone is full, it is flattened off at the top using the rod. Excess concrete at the base of the cone is removed to prevent from interfering with the test. At this point, the cone is slowly lifted upwards. The slump is then measured with a measuring tape from the top surface of the concrete to the top of the cone. The desired range for slump is 4” – 8”. If the concrete slump is too low, more HRWR is added to increase workability. Once slump is deemed sufficient, air content is then measured.

Similarly, air content is determined in compliance to ASTM C231. First, the bowl and device are moistened with water. Concrete is then added in the bowl in third by volume. Similar to the slump test, the layers are rodded 25 times, penetrating the previous

layer by 1 inch. In addition to the rodding, the bowl is struck with a mallet around its circumference after being rodded. Once the third layer is rodded and struck with a mallet, the top surface is leveled off with a trowel. The pressure device is then attached and clamped to the bowl. Water is pumped into one of the petcocks until water comes out of the other petcock. The valves are then closed and pumped until the pressure in the device is at the initial reading. At this point, a mallet is used to strike the bowl as the pressure is released. The air content is then read from the device. Similar to slump, the desired air content is 4 - 8%. If air content is not satisfactory, more AEA is added and the test is then repeated.

Figures 3.4 & 3.5 – Slump cone & Air meter for fresh property tests

3.3.3 Sampling and Curing

The sample size for each mix includes 35 4” – 8” cylinders, 3 4” x 4” x 11” free shrinkage prisms, 4 3” x 3” x 12” flexure prisms, and 2 AASHTO PP-34 restrained shrinkage rings. One of the rings is modified to allow for VWSG to be attached to the ring at the time of drying. The total volume of each mix is 4.48 cubic feet.

After mixing, each sample is casted according to their respective standards. Concrete is poured into the cylinders halfway and rodded 25 times. The cylinder is then struck with a mallet around its circumference to close any air voids. Once the last layer is poured, the top surface of the cylinder is leveled with a trowel. Caps are then put on top of the cylinders to prevent moisture from escaping. The same process is repeated with the free shrinkage and flexure prisms. Rather than caps, the prisms are wrapped in plastic sheet. For the rings, concrete is poured inside into 3 separate layers. The ring is then rodded 75 times as suggested by the AASHTO PP-34 standard. The base of the mold is struck with a mallet after each layer is rodded. Once the third layer is finished, a level surface is achieved with a wet trowel. Plastic sheet is then placed on top of the ring surface. The samples are then stored inside an environmental chamber with a constant temperature of 74˚ F and constant humidity of 50%.

Figures 3.6 & 3.7 – AASHTO ring, cylindrical, flexure, and free shrinkage molds for typical mix

Figure 3.8 – Environmental chamber held at constant temperature of 74˚ and 50% humidity

After 24 hours, all of the samples are demolded. Four cylinders are taken and tested for compression, tension, and elastic modulus. Five cylinders are placed inside of a lime tank for testing of surface resistivity and rapid chloride permeability. The rest of the cylinders are then placed in a curing room held at 100% humidity. The free shrinkage prisms are demolded and measured for initial readings. Two flexure prisms are tested for rupture modulus. At this point, the free shrinkage prisms are placed in the lime tank and the remaining flexure prisms are placed in the same curing environment as the cylinders. For the rings, the 4 supports are stripped and the ring is lifted off its base. The cardboard sonotube mold is then stripped. The ring is then placed on top of a polyurethane sheet and

covered with wet burlap. The polyurethane sheet is then wrapped and held closed tightly as to prevent any moisture loss from the burlap. All the samples begin drying at an age of 14 days with the exception of the 5 cylinders in the lime tank. The burlap is removed from the rings and connected to the datalogger. The VWSGs are attached to the bolts and tightened to read the strain. The top surface of the ring is wrapped with tape and then melted paraffin wax is poured on the top surface to prevent drying. The tape is used to prevent wax from sliding down the sides of the ring. The bottom surface of the rings is sealed with silicone caulk to prevent moisture escaping from the bottom surface. With this set up, drying only occurs on the sides of the ring.

Figure 3.9 – Wet-curing of AASHTO ring specimen

The AASHTO standard recommends to cure the specimen for 1 day in order to induce a full depth macrocrack. Prior to this experiment, this procedure was implemented

and it was proven to have no effect on the microcracks at 28 and 56 days. The curing period of 14 days was simply chosen to imitate the curing age experienced by the concrete in slab-on-girder bridge decks.

3.4 Laboratory Testing

Laboratory testing is done over the course of 56 days to allow for complete data collection of each mix. The following tests are performed:

Test	Standard	Age
Compressive Strength	ASTM C39	1, 3, 7, 14, 28, 56 days
Tensile Strength	ASTM C496	1, 3, 7, 14, 28, 56 days
Modulus of Elasticity	ASTM C469	1, 3, 7, 14, 28, 56 days
Modulus of Rupture	ASTM C78	1, 28 days
Free Shrinkage – Wet Cured	ASTM C157	1, 7, 14-21, 28, 35, 42, 56 days
Restrained Shrinkage	AASHTO PP-34	28, 56 days
Surface Resistivity	AASHTO T 358	7, 14, 28, 56 days
Rapid Chloride Permeability	AASHTO T 277	28, 56 days

Table 3.5 – Summary of tests performed

3.4.1 Compressive Strength Testing

Compressive strength of the mixes is determined in accordance to ASTM C39. Compressive strength is determined at 1, 3, 7, 14, 28, and 56 days. For the test, a 4” x 8” cylinder is capped with a sulfur capping compound. This is to ensure the top and bottom surface of the cylinder is flat and the stress is distributed across a more uniform area. The cylinder is then placed into a 1 million-lb Forney machine and is loaded at a rate of 35 ± 7 psi until failure occurs. Two cylinders are tested to determine the compressive strength.

If the two data points are not reasonably close to one another, another cylinder is tested. The compressive strength is taken to be the average of all the cylinders tested with outliers removed.

Figure 3.10 – Forney testing machine used to for compression, tension, and elastic modulus tests

Figure 3.11 – Capped cylinder in testing machine

3.4.2 Tensile Strength Testing

Tensile strength of the mixes is determined in accordance to ASTM C496. The cylinders are placed horizontally in the same Forney machine used to determine the compressive strength. The specimens are then loaded at the appropriate rate until failure occurs. Failure is typically identified once a vertical crack occurs in the bottom of the cylinder. Mixes without fibers failed suddenly while mixes with fibers allowed for more residual stresses to be absorbed in the specimen. Once the max load is achieved and failure occurs, the test is concluded and the data is recorded.

Figure 3.12 – Tensile strength testing of samples with and without fibers

3.4.3 Modulus of Elasticity Testing

Modulus of elasticity is determined in accordance to ASTM C469. This test is performed after the compressive strength is determined in order to allow for appropriate loading. Two cylinders are capped using a sulfur capping compound to ensure an even surface. The cylinders are then placed inside of a modulus cage. Three bolts are placed in the bottom of the cage while two bolts are placed at the top. This is done to ensure the cylinder and cage deform together. The safety pins are then removed and the cylinder and cage are placed in the testing machine. The cylinder is pre-loaded to 40% of the compression strength to prevent any jumps in strain during testing. The cylinder is then unloaded and two distance measurements are taken from the cage. Following this, the cylinder is then loaded at equal increments with a max value less than 40% of the compressive strength. At equal loadings, the length change is collected from the modulus

cage. Two people are present during testing: one calling out the loads at equal increments and the other writing down the length change from the modulus cage. The test is then repeated again with the same cylinder. Another two tests are performed with a difference cylinder. The modulus of elasticity is then equated to be the average of all four tests coming from two difference cylinders.

Figure 3.13 – Test sample with modulus cage in testing machine

3.4.4 Modulus of Rupture Testing

All testing done for rupture modulus is done according to ASTM C78. The 12” prisms are first marked at the appropriate locations where the supports and loading occurs. The supports are located 1.5” from the edges while the point loads occur 3” away from the support. This essentially is a 4- point bending fixture. After the set-up is complete, the specimen is then loaded at a rate of 0.001 in/sec. Failure occurs when a large deformation is identified by the machine. For specimens without fibers, the prisms split completely in half, whereas specimens with fibers are monolithic with a visible crack between the point loads. The peak load is then recorded and used to calculate the modulus of rupture.

Figure 3.14 – Testing set-up for rupture modulus

Figure 3.15 – Tested fiber-reinforced flexure samples

3.4.5 Surface Resistivity and Rapid Chloride Permeability Testing

Surface resistivity testing is done in accordance to AASHTO T 358. It is used as a quick alternative to rapid chloride permeability testing. The test consists of a device with 4 equally spaced electrodes being pressed into the specimen. A constant current is sent into the outer electrodes with the corresponding voltage being measured by the inner electrodes. A more permeable specimen will record a lower voltage due to a low resistance against the current produced. For each test, the device is pressed into the device at 90º increments. With two full revolutions, a total of eight measurements is recorded for each cylinder. Two cylinders are tested every time data is to be collected. An average of both cylinders is used to compute the surface resistivity of each mix.

Figure 3.16 – Surface resistivity meter

Rapid chloride permeability testing is done in accordance to AASHTO T 277. This testing is critical to ensure proper durability of a concrete mix. In bridge slabs, permeability is critical as it delays corrosion of the top layer of reinforcement. HPC is known for its extremely low permeability, yet additions of fiber may increase it. The day before testing, a cylinder is removed from the lime-saturated tank and cut into 3 – 2" segments for the duration of the test. The 2" discs are then placed into a tank of water and vacuumed for a minimum of 1 hour and soaked for a minimum of 18 hours. After the soaking period, the discs are placed in cells and tightened to prevent any solutions from leaking. At this point, a 3% solution of NaCl is poured into the left side of the cell, while the right side of the cell is filled with 0.3N NaOH solution. The corresponding wires from the cells are then connected to a computer and logged for a period of 6 hours. The current

at the end of this 6 hours is recorded. A lower current corresponds to a less permeable specimen. A minimum of two specimens were tested for each mix at each test interval.

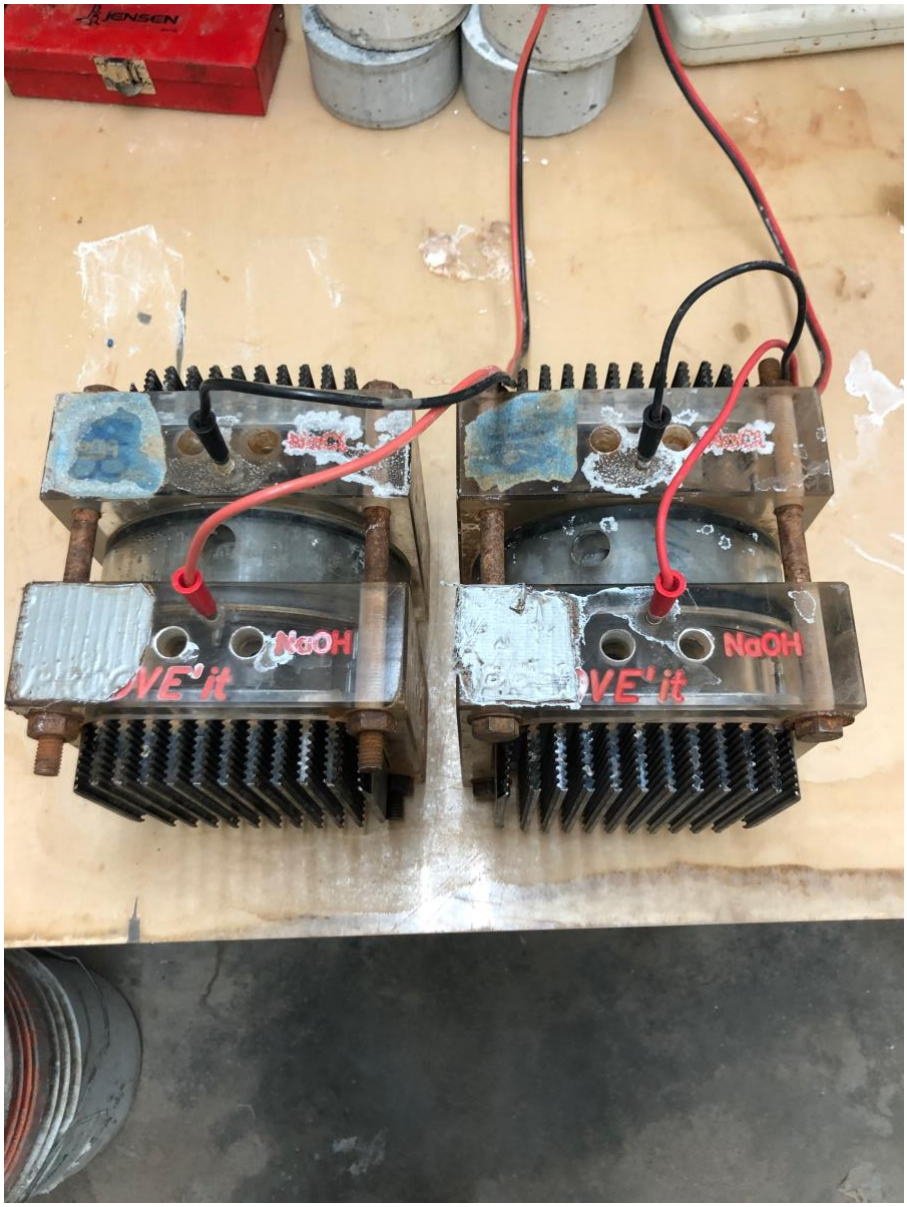

Figure 3.17 – Rapid chloride permeability cells

3.4.6 Free Shrinkage Testing

Free shrinkage testing is done in accordance to ASTM C157. Three 4” x 4” x 11” prisms are used for the duration of the test. After demolding, the prisms are then left with two studs on each side to allow for computation of length change. The initial readings are recorded and then tested whenever appropriate. After 14 days, the samples are moved to an environmental chamber held a constant temperature of 74 º F and relative humidity of 50%. To compute the length change, a rod of constant length is placed inside the length comparator and the number is recorded. After, the test specimen is placed inside the length comparator and this number is recorded. The difference of these two numbers is the primary focus of this test. As the prisms shrink, the difference of the two numbers decreases. It is critical to use the same rod for the entire duration of the test to ensure accurate readings. It is to be noted that any recordings done during the curing period typically resulted in swelling, where the specimen actually increases in size.

Figure 3.18 – Free shrinkage length comparator

3.4.7 Restrained Shrinkage Testing

The primary test that is utilized to measure cracking frequency properties is the AASHTO PP-34 ring test. The ring consists of an inner steel ring with 4 foil strain gauges attached with an outer surface of concrete. The inner steel ring is designed to restrain the concrete from shrinking. As a result, a hoop tensile stress is induced the ring. If this stress exceeds the tensile strength of the mix, the concrete cracks and the test is concluded. Age of cracking is identified with a relief of strain that is measured by the

steel ring. As stated in the AASHTO standard, any mix that does not develop a full crack within the testing period is deemed adequate for restrained shrinkage applications.

Figure 3.19 – AASHTO ring specimen with a visible full depth macrocrack

Figure 3.20 – Standard and modified AASHTO ring specimens

For every mix, two rings are produced. Both samples are wet cured with burlap for a period of 14 days. One ring will be the standard AASHTO ring with four foil strain gages attached on the inner side of the steel ring. The other ring will be a modified AASHTO ring with 6 VWSGs attached to the top surface of the ring. The AASHTO ring is good for determining age of cracking of concrete mixes but it does give any indication of the stress that is induced in the concrete itself. This modification is implemented to directly measure the strain that occurs in the concrete. With this set up, the steel ring can be used to predict age of cracking if any cracks occur, while the VWSGs can help predict the behavior of the stress that is induced in the concrete.

In addition to determining the age of cracking, the cracks are visually inspected, measured, and mapped. Since all of the mixes in this study do not develop full depth macro cracks, analysis of the microcracks is a critical part of this experiment. Microcrack mapping is done with the use of a portable Dinolite microscopic camera. The rings are scanned across the outer surface and the number of cracks are located. The crack mapper will circle the crack with a pencil so cracks can be located and analyzed at further ages. Typically, if the stress in the concrete is increasing, the crack width will also increase. Crack length is estimated based on the size of the drawn circle on the surface of the ring. Once the cracks are located and counted, the Dinolite software is used to take pictures of each crack. Along with the pictures, the cracks are mapped on pen and paper. Multiple pictures are taken of cracks longer than 1". Once the pictures are taken, the software is implemented to measure the widths of the cracks. Following this, analysis is done on the data collected to determine the number of cracks, average crack width, maximum crack width, as well as the crack area. These are the main parameters that will be used to determine cracking frequencies of each of the mixes.

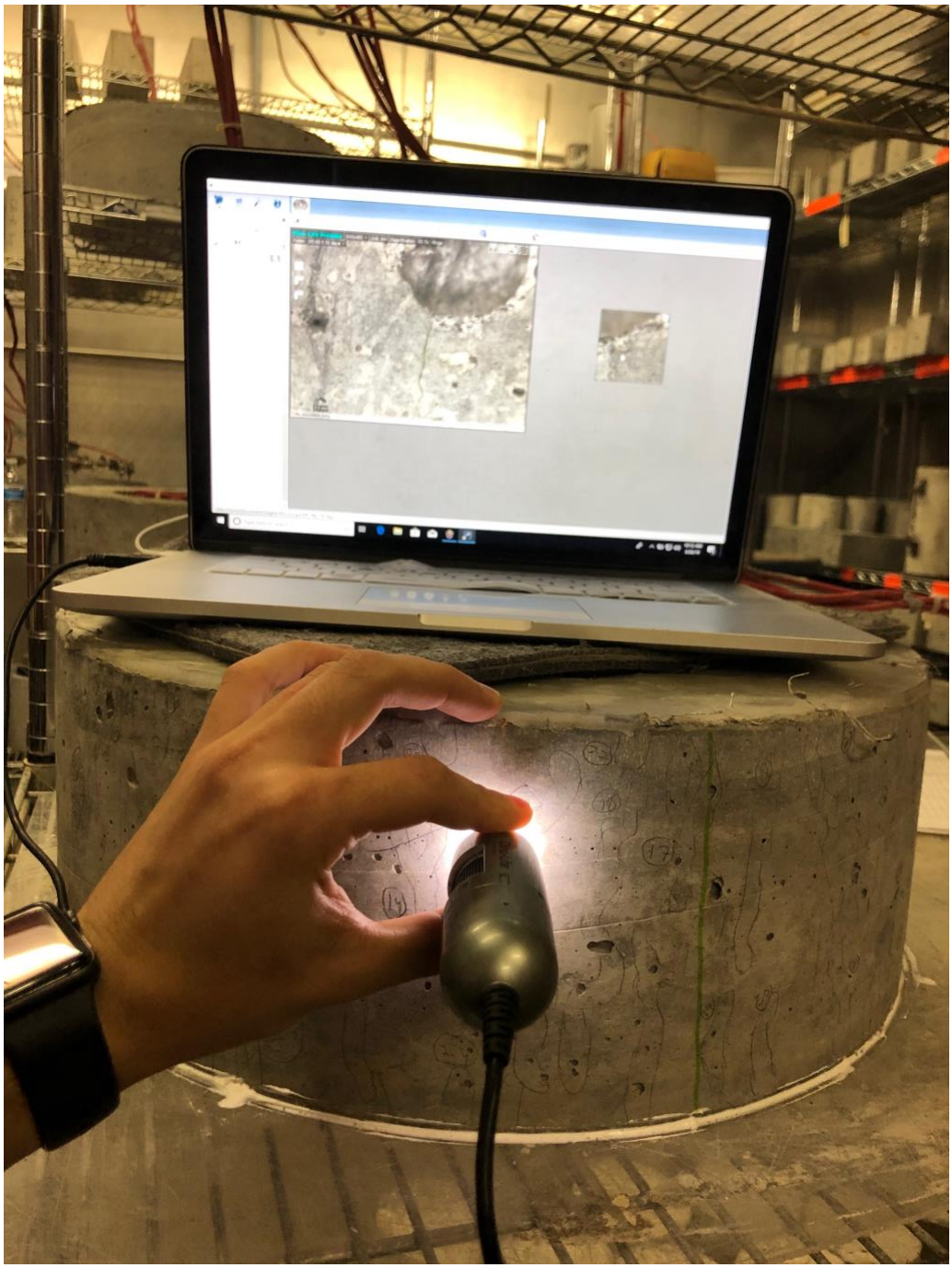

Figure 3.21 – Dinolite software used to measure crack widths found with microscopic camera

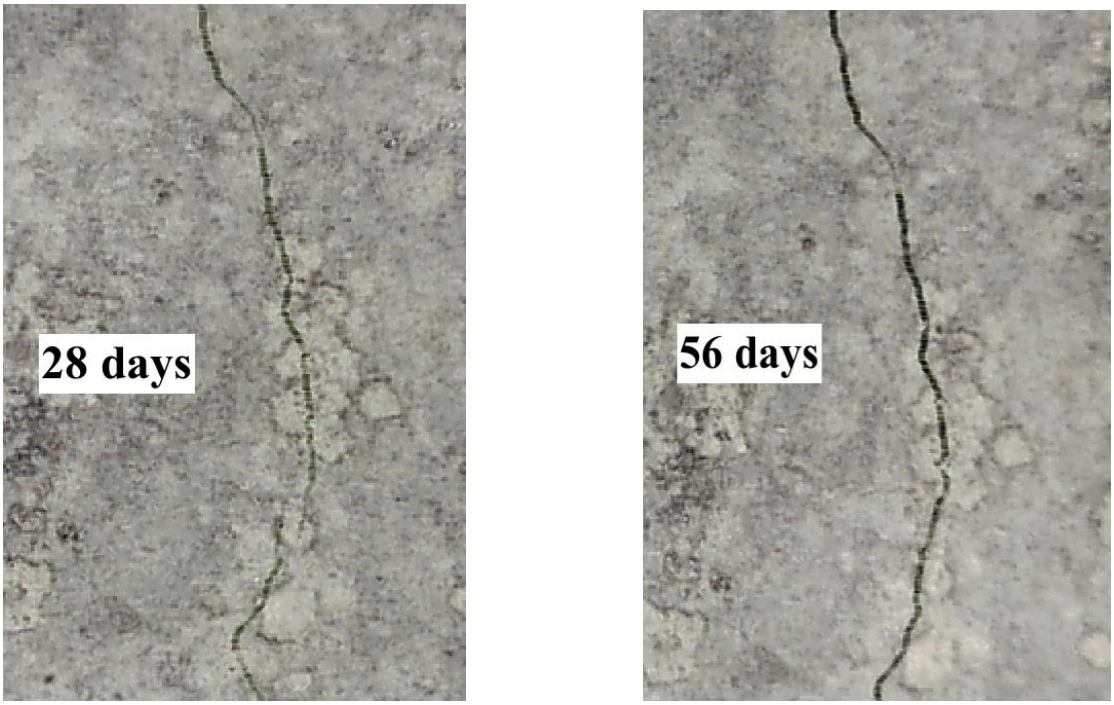

Figure 3.22 – Crack width growth between 28 and 56 days

3.4.7.1 Modified AASHTO Restrained Shrinkage Test

Along with the one sample that is casted according to the AASHTO PP-34 standard, another modified ring is implemented to further analyze the strain experienced by the concrete. It involves utilizing the hexagonal VWSG tool shown in Figure. After the top surface of the ring is flattened and smooth, the 6 steel bolts are embedded 1.5 in. into the concrete. Once demolded, the hexagonal tool is removed, leaving the 6 steel bolts exposed as shown in Figure. At this point, the VWSGs are tightened on top of these bolts to allow for strain measurement of the concrete.

Figure 3.23 – Hexagonal bolt tool to allow for VWSG instrumentation

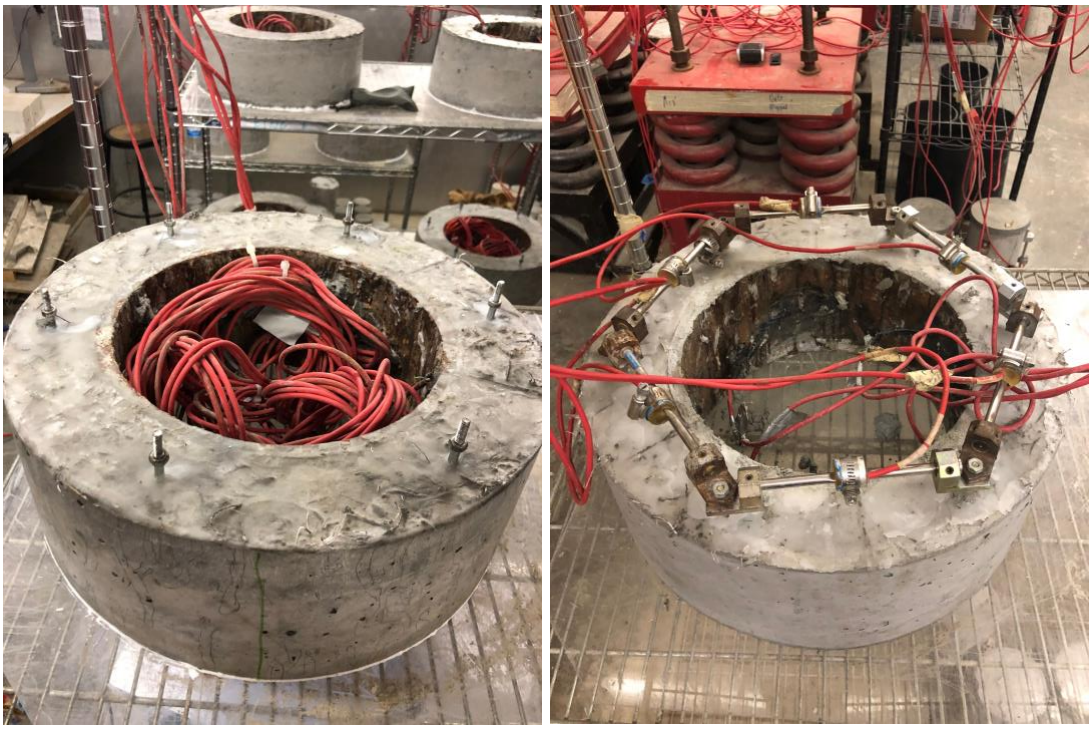

Figure 3.24 – Modified AASHTO ring specimen with VWSGs

The VWSG instrumentation has been successfully used in recent studies to better understand the age of cracking and the behavior of the concrete before and after cracking. Since the VWSGs provide the strain in the concrete, it will be compared to the cracking strain of the mix. The equation to calculate the cracking strain can be seen below.

$$\varepsilon_{crack} = \frac{\sigma_T}{E_C} \tag{3.1}$$

It is evident that a mix with a higher tensile strength, σ_T, and a lower modulus of elasticity, E_C, will require more strain in order to induce cracking. The VWSG data will also be compared to the FSG data collected from the steel ring. Both sets of data will give more insight on the stress accumulation in the concrete. Typically, when a ring develops a full depth crack, the both VWSGs and FSGs experience in an upward jump in strain. An example of this instrumentation done by Zeeshan Ghanchi in 2015 on polypropylene fiber-reinforced self-consolidating concrete can be seen in the figure below.

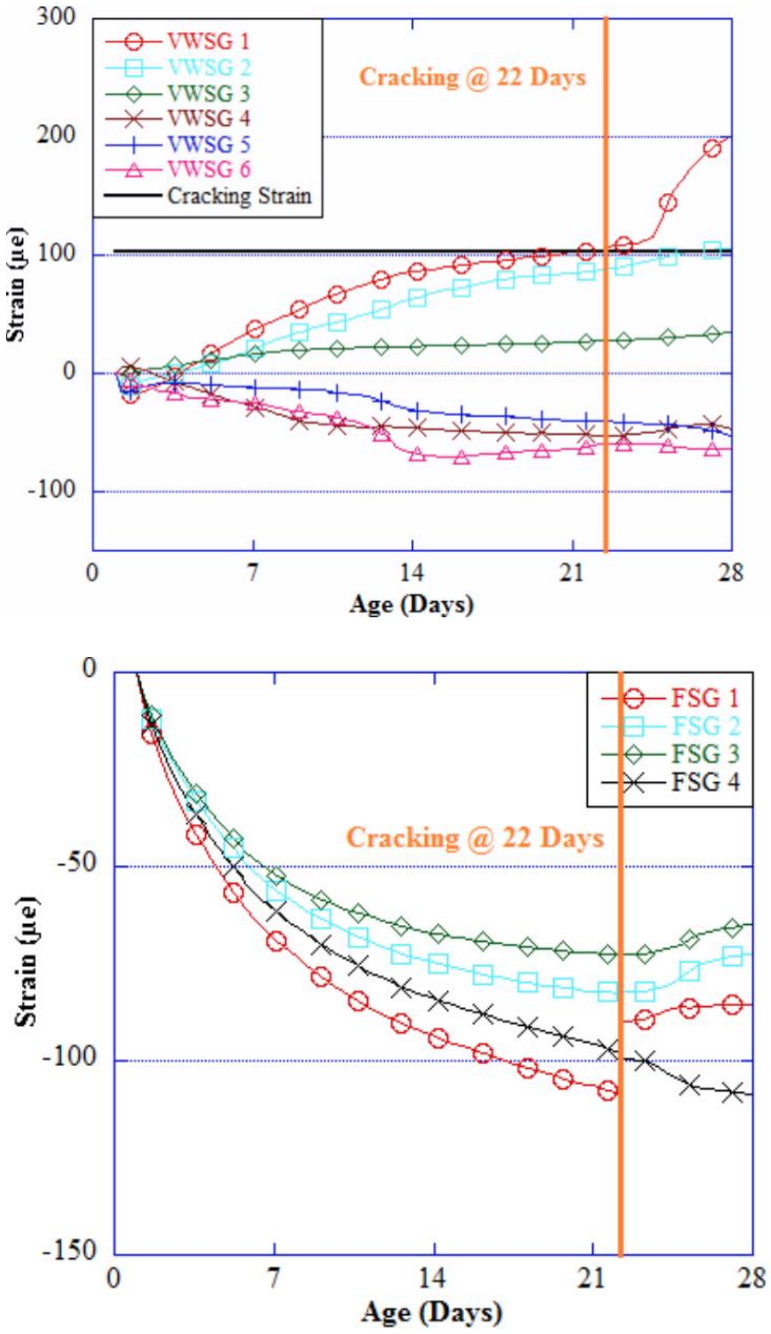

Figure 3.25 – Example of VWSG data used to determine age of cracking (Ghanchi 2015)

All mixes in this experiment consist of one modified AASHTO specimen. Since none of the mixes develop a full-depth crack, the VWSG data is not as critical as the crack-mapping data. Age of cracking is not an important parameter in this study.

It is important to note that the parameters measured using this procedure is only used as a tool to compare various concrete mixes. It does not give any indication as to how mixes will perform and crack in the field.

4. Results

4.1 Introduction

This experiment is aimed to investigate any benefits of implementing hybrid fibers. This study will consist of 5 hybrid mixes with varying fiber types and dosages. Two more mixes will be reinforced with one type of fiber and will be used as control mixes. An additional mix without fibers is also included in this research to further investigate the effects of fiber addition. All mix designs in this study are identical with the varying parameter being fiber content.

For each mix, 35 cylinders are casted for various testing of mechanical properties and permeability tests. In addition, 3 free shrinkage prisms are casted along with 4 flexure prisms. Two AASHTO rings are also casted, one standard ring and one modified ring to allow for instrumentation of VWSGs. All samples are demolded after 24 hours and are wet cured for a period of 14 days. After curing, all samples are stored an environmental chamber at a temperature of 74˚ F and 50% humidity. Table 4.1 summarizes the mixes that are under investigation.

Mix ID	$M^0N^0S^0$	$M^0N^0S^{42}$	$M^5N^0S^0$	$M^{2.5}N^{0.5}S^0$	$M^5N^{0.5}S^0$	$M^0N^{0.5}S^{12.5}$	$M^5N^0S^5$	$M^5N^0S^7$
Macro Fibers (lb/cy)	-	-	5	2.5	5	-	5	5
Micro Fibers (lb/cy)	-	-	-	0.5	0.5	0.5	-	
Steel Fibers (lb/cy)	-	42	-	-	-	12.5	5	7

Table 4.1 – Summary of mix designs with varying fiber doses

- Two hybrid mixes will consist of macro and micro fibers ($M^{2.5}N^{0.5}S^0$ & $M^5N^{0.5}S^0$)
- One hybrid mix will consist of steel and micro fibers ($M^0N^{0.5}S^{12.5}$)
- Two hybrid mixes will consist of steel and macro fibers ($M^5N^0S^5$ & $M^5N^0S^7$)
- Two control mixes will consist of one type of fiber ($M^5N^0S^0$ & $M^0N^0S^{42}$)
- An additional control mix will consist no fibers ($M^0N^0S^0$)

4.2 Fresh Properties

The fresh properties of this research consist of air and slump tests. Slump testing is done in accordance to ASTM C143 while air testing is done in accordance to ASTM C231. The mixing is done at a constant room temperature so concrete temperature is not measured. One thing to note is that varying amounts of superplasticizer is used to compensate for loss of workability with the addition of fibers. Table 4.2 summarizes the fresh property results of each mix.

Mix ID	$M^0N^0S^0$	$M^0N^0S^{42}$	$M^5N^0S^0$	$M^{2.5}N^{0.5}S^0$	$M^5N^{0.5}S^0$	$M^0N^{0.5}S^{12.5}$	$M^5N^0S^5$	$M^5N^0S^7$
HRWR (oz/cwt)	4.4	4	5.3	5.3	4.9	4.9	4.9	4.9
AEA (oz/cwt)	0.125	0.125	0.125	0.125	0.125	0.125	0.125	0.125
Slump (in.)	5”	5.5”	3.5”	5”	4”	7”	5.5”	3.5”
Air content (%)	4.5%	4.5%	4%	5%	4.8%	4.5%	4.5%	4%

Table 4.2 – Summary of fresh property results

The most critical parameter with implementing fibers in a concrete mix is the reduction of workability. Less workability is associated with higher labor costs due to increased time of pouring. Hence, it is vital to investigate the slump reduction of each mix. Based on Table 4.2, a moderate reduction of slump is identified when any amount of fibers is utilized, depending on the dose. Macro fibers tend to reduce workability more than steel fibers. This may be attributed to the fiber size (2” for macro and 1.5” for steel). Higher doses of fibers are associated with a higher reduction of slump, so more superplasticizer is added if it is needed. In addition, by inspection of Table 4.2, it can be concluded that fibers do not have any effect on air content. Perhaps the fiber content is too low to have any effect. In conclusion, mixes with fibers will require higher amounts of superplasticizer which may be a cost consideration if large amounts of fiber-reinforced concrete are to be produced.

4.3 Mechanical Properties

The mechanical properties under investigation are compressive strength, modulus of elasticity, tensile strength, modulus of rupture, surface resistivity, and rapid chloride permeability. These tests are all conducted in accordance to their respective ASTM standards. All tests are done to identify any effects produced with the addition of hybrid fibers.

4.3.1 Compressive Strength

Compressive strength is determined at 1, 3, 7, 14, 28, and 56 days. A minimum of two 4" x 8" cylinders are tested at each age. If any outliers are present, another cylinder is tested. A summary of the results can be seen in Table 4.3 and graph of the strength over time can be seen in Figure 4.1. The first, second, and third percentages in each cell represent the increase or decrease in compressive strength with respect to $M^0N^0S^0$, $M^0N^0S^{42}$, and $M^5N^0S^0$ respectively

Age	$M^0N^0S^0$		$M^0N^0S^{42}$		$M^5N^0S^0$		$M^{2.5}N^{0.5}S^0$		$M^5N^{0.5}S^0$		$M^0N^{0.5}S^{12.5}$		$M^5N^0S^5$		$M^5N^0S^7$	
1	3069	-	3404	10.9%	3718	21.1%	3439	12.1%	3909	27.4%	3682	20.0%	3666	19.5%	3503	14.1%
		-9.8%		-		9.2%		1.0%		14.8%		8.2%		7.7%		2.9%
		-17.5%		-8.4%		-		-7.5%		5.1%		-1.0%		-1.4%		-5.8%
3	N/A	-	N/A	-	N/A	-	4837	-	4618	-	N/A	-	4587	-	N/A	-
		-		-		-		-		-		-		-		-
		-		-		-		-		-		-		-		-
7	4916	-	5285	7.5%	5772	17.4%	5971	21.5%	5673	15.4%	5314	8.1%	5643	14.8%	5374	9.3%
		-7.0%		-		9.2%		13.0%		7.3%		0.5%		6.8%		1.7%
		-14.8%		-8.4%		-		3.4%		-1.7%		-7.9%		-2.2%		-6.9%
14	5812	-	6310	8.6%	6748	16.1%	6170	6.2%	6280	8.1%	6449	11.0%	6409	10.3%	5852	0.7%
		-7.9%		0.0%		6.9%		-2.2%		-0.5%		2.2%		1.6%		-7.3%
		-13.9%		-6.5%		-		-8.6%		-6.9%		-4.4%		-5.0%		-13.3%
28	7707	-	7630	-1.0%	7635	-0.9%	7962	3.3%	8201	6.4%	7604	-1.3%	7962	3.3%	7767	0.8%
		1.0%		-		0.1%		4.4%		7.5%		-0.3%		4.4%		1.8%
		0.9%		-0.1%		0.0%		4.3%		7.4%		-0.4%		4.3%		1.7%
56	8221	-	8838	7.5%	8519	3.6%	8041	-2.2%	8917	8.5%	8333	1.4%	9076	10.4%	8559	4.1%
		-7.0%		-		-3.6%		-9.0%		0.9%		-5.7%		2.7%		-3.2%
		-3.5%		3.7%		-		-5.6%		4.7%		-2.2%		6.5%		0.5%

Table 4.3 – Compressive strength results

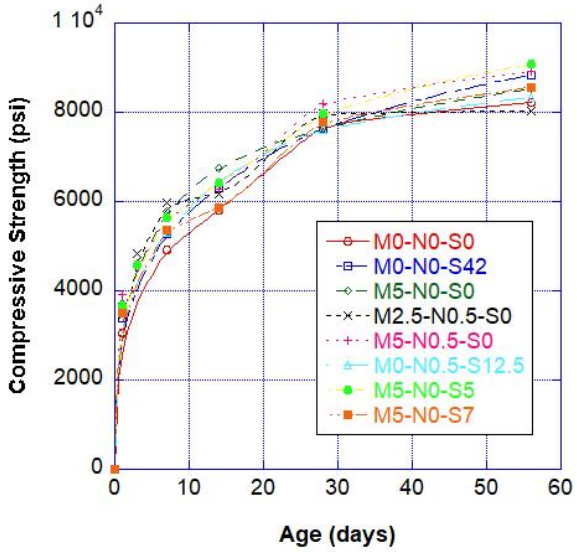

Figure 4.1 – Compressive strength vs. time

By inspection of Table 4.3, a few observations can be made. The addition of fibers tends to increase compressive strength at early ages. All of the hybrid mixes provide an increase in compressive strength at 1 day, with $M^5N^{0.5}S^0$ providing the highest increase of 27.4% in comparison to the control mix without fibers. This increase may be a result of the fibers intercepting cracks as they occur. As the specimens age, this increase becomes less apparent. All of the mixes have a water to binder ratio of 0.382 and, as a result, the compressive strength at 28 days is held constant. Therefore, it can be concluded that hybrid fibers do not negatively impact compressive strength with fiber volumes ranging less than 0.37%. In fact, they increase compressive strength at early ages.

4.3.2 Splitting Tensile Strength

A critical parameter that is affected with the addition of fibers is tensile strength. It is important to investigate the impact of each type of fiber on tensile strength. Tensile strength is determined at day 1, 3, 7, 14, 28, and 56 days. Two 4” x 8” cylinders are loaded horizontally in accordance to ASTM C496. Once the max load is achieved, the data is collected and the tensile strength is calculated. The table below summarizes the results.

Age	$M^0N^0S^0$		$M^0N^0S^{42}$		$M^5N^0S^0$		$M^{2.5}N^{0.5}S^0$		$M^5N^{0.5}S^0$		$M^0N^{0.5}S^{12.5}$		$M^5N^0S^5$		$M^5N^0S^7$	
1	347	-	421	21.3%	444	28.0%	402	15.9%	417	20.2%	356	2.6%	400	15.3%	443	27.7%
		-17.6%		-		5.5%		-4.5%		-1.0%		-15.4%		-5.0%		5.2%
		-21.8%		-5.2%		-		-9.5%		-6.1%		-19.8%		-9.9%		-0.2%
3	N/A	-	N/A	-	N/A	-	468	-	499	-	N/A	-	445	-	N/A	-
		-		-		-		-		-		-		-		-
		-		-		-		-		-		-		-		-
7	450	-	513	14.0%	487	8.2%	500	11.1%	504	12.0%	563	25.1%	535	18.9%	516	14.7%
		-12.3%		-		-5.1%		-2.5%		-1.8%		9.7%		4.3%		0.6%
		-7.6%		5.3%		-		2.7%		3.5%		15.6%		9.9%		6.0%
14	536	-	549	2.4%	550	2.6%	584	9.0%	541	0.9%	547	2.1%	556	3.7%	527	-1.7%
		-2.4%		-		0.2%		6.4%		-1.5%		-0.4%		1.3%		-4.0%
		-2.5%		-0.2%		-		6.2%		-1.6%		-0.5%		1.1%		-4.2%
28	599	-	575	-4.0%	608	1.5%	629	5.0%	625	4.3%	603	0.7%	633	5.7%	583	-2.7%
		4.2%		-		5.7%		9.4%		8.7%		4.9%		10.1%		1.4%
		-1.5%		-5.4%		-		3.5%		2.8%		-0.8%		4.1%		-4.1%
56	617	-	619	0.3%	668	8.3%	732	18.6%	673	9.1%	661	7.1%	661	7.1%	619	0.3%
		-0.3%		-		7.9%		18.3%		8.7%		6.8%		6.8%		0.0%
		-7.6%		-7.3%		-		9.6%		0.7%		-1.0%		-1.0%		-7.3%

Table 4.4 – Splitting tensile strength results

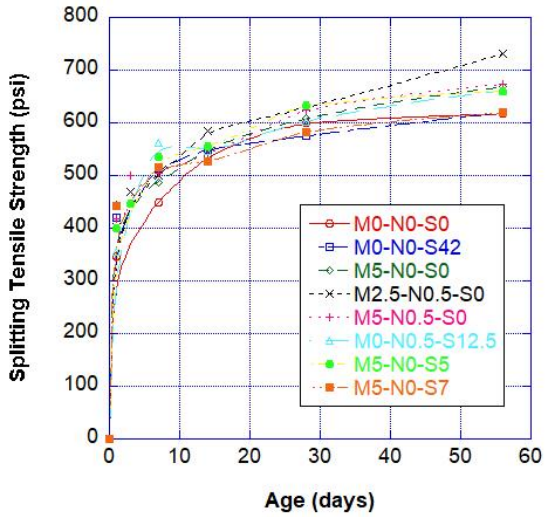

Figure 4.2 – Splitting tensile strength vs. time

The first clear conclusion that can be made is that all mixes with fibers increase tensile strength at almost all ages in comparison to the control mix without fibers. At 56 days, an 8.3% increase is seen in $M^5N^0S^0$ in comparison to the control mix without fibers. One of the main objectives of this study is to improve the tensile strength of $M^5N^0S^0$ by implementing hybrid fibers. $M^{2.5}N^{0.5}S^0$ and $M^5N^{0.5}S^0$ both provide an increase of 18.3% and 8.7% respectively in tensile strength in comparison to $M^5N^0S^0$. This provides definitive evidence that hybrid combinations of macro and micro fibers provide a higher resistance to tension in comparison to macro fibers alone. This can be attributed to the synergy effect that is created when macro fibers are combined with micro fibers.

Another conclusion that can be made is that $M^5N^0S^5$ provides a higher tensile strength in comparison to $M^5N^0S^7$. This may suggest that $M^5N^0S^7$ has too many fibers, and as a result, it compromises the tensile integrity of the concrete. However, $M^5N^0S^5$ does not provide any improvement in tensile strength in comparison to $M^5N^0S^0$.This suggests that combining macro fibers and steel fibers does not create any synergy in comparison to macro fibers alone.

4.3.3 Modulus of Elasticity

Modulus of elasticity is determined at 1, 3, 7, 14, 28, and 56 days. The cylinders are first capped using a sulfur cement capping compound according to ASTM C617. Then, the elastic modulus is determined in accordance to ASTM C469. Table 4.4 summarizes the results below. Figure 4.2 shows the modulus of elasticity over time.

Age	$M^0N^0S^0$		$M^0N^0S^{42}$		$M^5N^0S^0$		$M^{2.5}N^{0.5}S^0$		$M^5N^{0.5}S^0$		$M^0N^{0.5}S^{12.5}$		$M^5N^0S^5$		$M^5N^0S^7$	
1	4246	-	4263	0.4%	4818	13.5%	4492	5.8%	4692	10.5%	4444	4.7%	4391	3.4%	4256	0.2%
		-0.4%		-		13.0%		5.4%		10.1%		4.2%		3.0%		-0.2%
		-11.9%		-11.5%		-		-6.8%		-2.6%		-7.8%		-8.9%		-11.7%
3	N/A	-	N/A	-	N/A	-	5146	-	4619	-	N/A	-	4605	-	N/A	-
		-		-		-		-		-		-		-		-
		-		-		-		-		-		-		-		-
7	4957	-	4925	-0.6%	5286	6.6%	4867	-1.8%	4940	-0.3%	4549	-8.2%	4829	-2.6%	4567	-7.9%
		0.6%		-		7.3%		-1.2%		0.3%		-7.6%		-1.9%		-7.3%
		-6.2%		-6.8%		-		-7.9%		-6.5%		-13.9%		-8.6%		-13.6%
14	4795	-	4928	2.8%	5123	6.8%	4572	-4.7%	4821	0.5%	4973	3.7%	4756	-0.8%	4932	2.9%
		-2.7%		-		4.0%		-7.2%		-2.2%		0.9%		-3.5%		0.1%
		-6.4%		-3.8%		-		-10.8%		-5.9%		-2.9%		-7.2%		-3.7%
28	4996	-	4848	-3.0%	4990	-0.1%	4764	-4.6%	4724	-5.4%	5225	4.6%	4945	-1.0%	4940	-1.1%
		3.1%		-		2.9%		-1.7%		-2.6%		7.8%		2.0%		1.9%
		0.1%		-2.8%		0.0%		-4.5%		-5.3%		4.7%		-0.9%		-1.0%
56	4607	-	4908	6.5%	4553	-1.2%	4515	-2.0%	4577	-0.7%	4754	3.2%	4632	0.5%	4572	-0.8%
		-6.1%		-		-7.2%		-8.0%		-6.7%		-3.1%		-5.6%		-6.8%
		1.2%		7.8%		-		-0.8%		0.5%		4.4%		1.7%		0.4%

Table 4.5 – Modulus of elasticity results

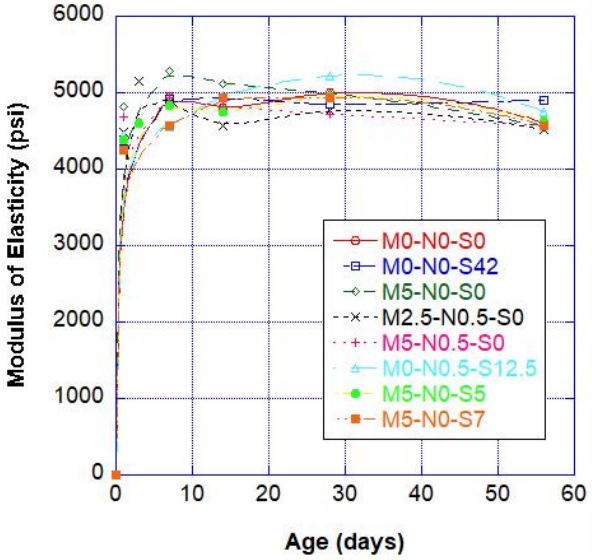

Figure 4.3 – Modulus of elasticity vs. time

From inspection of Table 4.4, it can be concluded that at 56 days, fiber additions, including hybrid combinations, do not have any significant effect on the elastic modulus. $M^0N^0S^{42}$ provides the highest modulus of elasticity at 56 days, providing an increase of 6.5% in comparison to the control mix without fibers. This can be attributed to the fact that steel fibers have a much higher elastic modulus in comparison to concrete. All mixes display a similar trend: a low modulus of elasticity on day 1 that increases significantly up to day 7. After this, a small decrease is observed as the concrete ages, which is a result of the addition of silica fume. In conclusion, the modulus of elasticity is not significantly affected with the addition of any fibers, but steel fibers provide a slight increase of 6.5% in comparison to the control mix without any fibers.

4.3.4 Modulus of Rupture

Another crucial parameter that is strongly affected by the addition of fibers is the modulus of rupture. This, in essence, is the tensile strength of concrete under flexural bending. Increasing this value will provide concrete with the ability to crack at a higher stress when subjected to bending. This is very important when induced tensile stresses are created. Rupture modulus is determined at day 1 and 28. A summary of the results can be seen in Table 4.6.

Age	$M^0N^0S^0$		$M^0N^0S^{42}$		$M^5N^0S^0$		$M^{2.5}N^{0.5}S^0$		$M^5N^{0.5}S^0$		$M^0N^{0.5}S^{12.5}$		$M^5N^0S^5$		$M^5N^0S^7$	
1	532	-	589	10.7%	596	12.0%	592	11.3%	553	3.9%	549	3.2%	633	19.0%	553	3.9%
		-9.7%		-		1.2%		0.5%		-6.1%		-6.8%		7.5%		-6.1%
		-10.7%		-1.2%		-		-0.7%		-7.2%		-7.9%		6.2%		-7.2%
28	603	-	610	1.2%	655	8.6%	679	12.6%	678	12.4%	751	24.5%	722	19.7%	678	12.4%
		-1.1%		-		7.4%		11.3%		11.1%		23.1%		18.4%		11.1%
		-7.9%		-6.9%		-		3.7%		3.5%		14.7%		10.2%		3.5%

Table 4.6 – Summary of modulus of rupture results

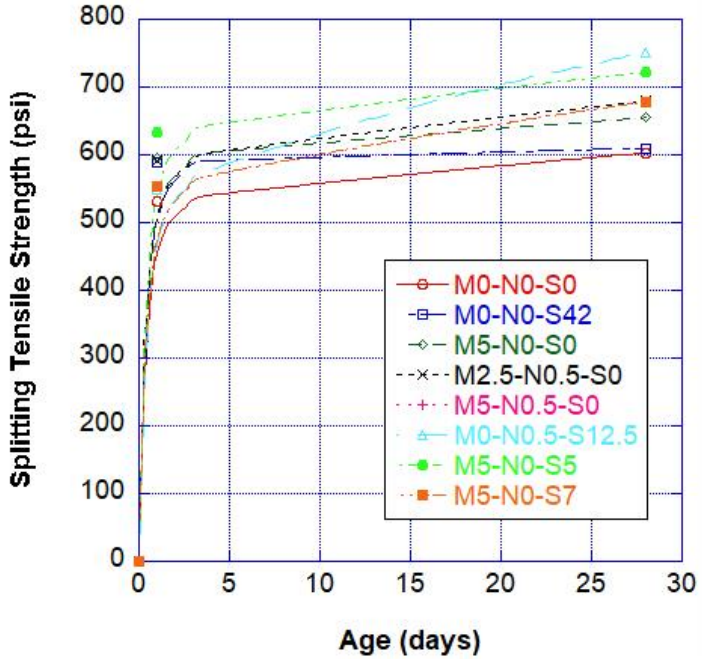

Figure 4.4 – Modulus of rupture vs. time

From inspecting of Table 4.6, a few conclusions can be made. First, all mixes with fibers have a higher rupture modulus in comparison to $M^0N^0S^0$. In addition, $M^{2.5}N^{0.5}S^0$ and $M^0N^{0.5}S^{12.5}$ provide an increase of 6.7% and 14.7% respectively in rupture modulus in comparison to $M^5N^0S^0$ at 28 days. The tensile reduction of $M^5N^0S^7$ against $M^5N^0S^5$ is confirmed with the rupture modulus results. $M^5N^0S^5$ continues to be the optimal dose for macro and steel fibers. In conclusion, $M^0N^{0.5}S^{12.5}$ provides the highest benefit for modulus of rupture, providing an increase of 24.5% against $M^0N^0S^0$.

4.4 Surface Resistivity and Rapid Chloride Permeability

Surface resistivity is done in order to quickly assess the permeability of each mix. It is done using a device consisting of 4 electric probes. SR is evaluated at day 7, 14, 28, and 56 days. A higher value corresponds to a lower permeability. A summary of the results is presented in Table 4.7.

Age	$M^0N^0S^0$	$M^0N^0S^{42}$	$M^5N^0S^0$	$M^{2.5}N^{0.5}S^0$	$M^5N^{0.5}S^0$	$M^0N^{0.5}S^{12.5}$	$M^5N^0S^5$	$M^5N^0S^7$
7	12.3	9.4	11.8	11.4	11.8	10.5	8.9	10.1
14	19.1	14.5	18.4	17.8	19.1	18.5	12.2	12.7
28	38.3	22.8	30.7	31.3	31.9	30.5	17.9	19.3
56	66.8	40.2	62.0	53.6	58.7	52.8	31.0	27.9

Table 4.7 – Summary of surface resistivity results (kOhm-cm)

$M^0N^0S^0$ performs the best in terms of permeability. This is expected because of HPC's curing rates and low permeability properties. The addition of fibers is expected to increase permeability, and the results confirm this prediction. By looking at Table 4.7, it can be seen that steel fibers increased permeability significantly, much more than macro and micro fibers. Polypropylene fibers tend to increase permeability, but to a much lesser extent. At 56 days, $M^5N^{0.5}S^0$ increased surface resistivity by 5.3% in comparison to

$M^5N^0S^0$. It is unclear whether this is due to the hybrid combination of fibers or an increase in total fiber content by volume. Regardless, this minor increase is negligible.

One important thing to note is when macro fibers are combined with steel fibers, a significant increase in permeability is seen. This may be attributed to both the conducting nature of steel fibers and an increase in fiber content. This is confirmed with results from $M^5N^0S^5$, $M^5N^0S^7$, and $M^0N^0S^{42}$. In conclusion, hybrids of macro and micro fibers increase permeability to a slight degree, whereas hybrids consisting of macro and steel display a significant increase in permeability.

Another test that is performed in this study to confirm permeability results is the rapid chloride permeability test. It is done at ages 28 and 56 days. Results from this test and SR will be used to evaluate the overall permeability of each mix. A lower value corresponds to a lower permeability. A summary of the results is presented in Table 4.8

Age	$M^0N^0S^0$	$M^0N^0S^{42}$	$M^5N^0S^0$	$M^{2.5}N^{0.5}S^0$	$M^5N^{0.5}S^0$	$M^0N^{0.5}S^{12.5}$	$M^5N^0S^5$	$M^5N^0S^7$
28	990	2681	1244	1697	1480	1735	2584	2893
56	771	1428	834	1088	790	1170	1753	1952

Table 4.8 – Summary of rapid chloride permeability results (coulombs)

As concluded earlier from the surface resistivity results, $M^0N^0S^0$ performs the best in terms of permeability. In addition, when adding only macro fibers, a slight reduction in permeability is observed. As stated earlier, hybrids consisting of macro and micro fibers provide a slight increase in permeability in comparison to the control mix with just macro fibers. The rapid chloride permeability results confirm the fact that when combining macro and steel fibers, a significant increase in permeability is seen. Therefore, in conclusion, hybrids provide a slight increase in permeability, yet ones that consist with steel fibers show a critical increase in permeability.

4.5 Free Shrinkage

Free shrinkage is a critical parameter when assessing mixes subjected to restrained conditions. A mix that has a higher free shrinkage will ultimately shrink more under restraint. Many factors provide restraint in a bridge deck, like reinforcement, steel decking, etc. Restraint is inevitable, therefore choosing a mix design that provides less shrinkage is vital. The samples in this study are wet-cured for 14 days, the same period that bridge decks are cured for. This is done to provide an accurate representation in the lab of what occurs in the field. A table of the 56-day free shrinkage results is presented in Table 4.9.

Mix ID	56-day free shrinkage (με)	± % w.r.t. $M^0N^0S^0$, $M^{42}N^0S^0$, $M^5N^0S^0$
$M^0N^0S^0$	270	-
		22.7%
		1.9%
$M^0N^0S^{42}$	220	-18.5%
		-
		-17.0%
$M^5N^0S^0$	265	-1.9%
		20.5%
		-
$M^{2.5}N^{0.5}S^0$	250	-7.4%
		13.6%
		-5.7%
$M^5N^{0.5}S^0$	210	-22.2%
		-4.5%
		-20.8%
$M^0N^{0.5}S^{12.5}$	247.5	-8.3%
		12.5%
		-6.6%
$M^5N^0S^5$	240	-11.1%
		9.1%
		-9.4%
$M^5N^0S^7$	235	-13.0%
		6.8%
		-11.3%

Table 4.9 – 56-day free shrinkage results

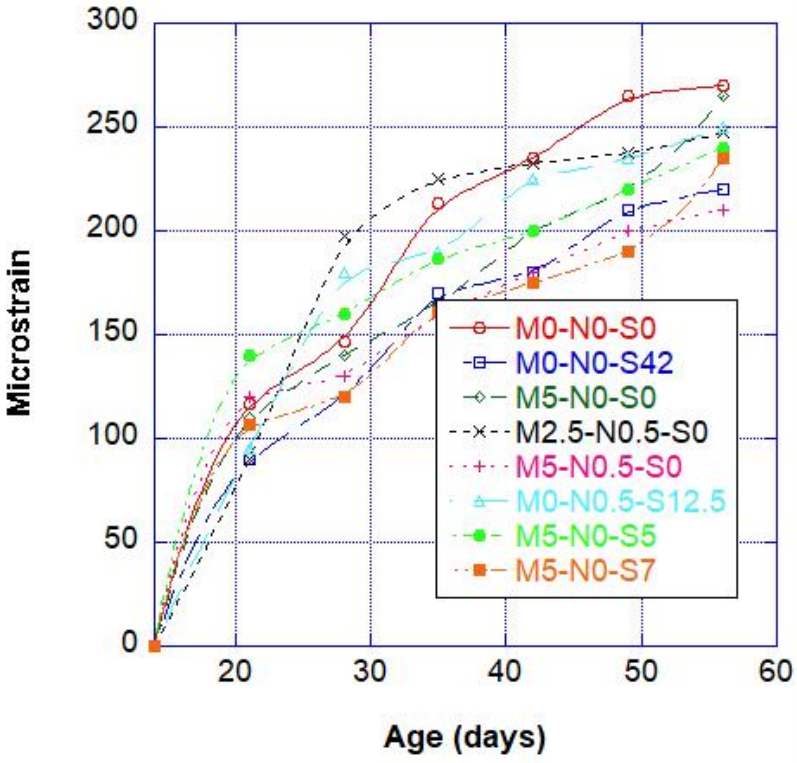

Figure 4.5 – Free shrinkage vs. time

By inspecting Table 4.9 and Figure 4.5, a few conclusions can be made. First, $M^0N^0S^0$ has the highest free shrinkage at 56 days. This suggests that any fiber addition and combination has potential to reduce free shrinkage. $M^0N^0S^{42}$ reduces free shrinkage by 18.5% in comparison to the control mix without fibers, suggesting that steel fibers tend to reduce free shrinkage. As stated previously, improving $M^5N^0S^0$ is one of the primary objectives of this experiment. $M^{2.5}N^{0.5}S^0$ and $M^5N^{0.5}S^0$ reduce free shrinkage by 5.7% and 20.8% respectively in comparison to $M^5N^0S^0$. This may be attributed to the possibility that micro fibers reduce free shrinkage. In conclusion, hybrids consisting of macro and micro fibers reduce the free shrinkage experienced by macro fibers alone, suggesting that micro fibers tend to reduce volume change in concrete.

4.6 Restrained Shrinkage

In addition to free shrinkage, the AASHTO PP-34 ring test is implemented to further analyze restrained shrinkage properties of each mix. This test is the main focus of this study and many parameters are under investigation. Two rings are produced for each mix, one standardized AASHTO ring and one modified ring. Both rings are crack mapped at 28 and 56 days completely for data collection and verification. The ring test allows for full analysis to the effect of fibers on cracking under restrained conditions.

The main parameters examined using the crack mapping data are number of cracks, cracking area, average crack width, and maximum crack width. Although the main objective of the ring test is to induce full depth cracking to allow for comparison of the age of cracking, all of the rings done in this study never develop a full depth crack. This is why crack mapping is crucial in analyzing each mix.

In addition to the crack mapping, strain data is collected from each mix from the inner steel ring. The purpose of the strain data is to determine the age of cracking, but with Weiss's equation described earlier, the strain data can be used to evaluate the stress in the concrete itself. The VWSG data was not sufficient enough to compare to this data. Therefore, the theoretical stress calculated in the concrete will be compared to the experimental tensile strength, allowing for full evaluation of each mix.

4.6.1 $M^0N^0S^0$

	Number of Cracks	Average Crack Width (in)	Maximum Crack Width (in)	Cracking Area (in^2)	Age of Cracking (days)
Ring 1	122	0.000660	0.00177	0.1397	TBD
Ring 2	117	0.000646	0.00133	0.1406	TBD
Average	**120**	**0.000653 σ = 0.000233**	**0.00177**	**0.1402**	**-**

Table 4.10 $M^0N^0S^0$ 28-day crack mapping results

	Number of Cracks	Average Crack Width (in)	Maximum Crack Width (in)	Cracking Area (in^2)	Age of Cracking (days)
Ring 1	146	0.000691	0.00189	0.1631	None
Ring 2	134	0.000724	0.00142	0.1731	None
Average	**140**	**0.000708 σ = 0.000275**	**0.00189**	**0.1681**	**-**

Table 4.11 $M^0N^0S^0$ Ring 56-day crack mapping results

This mix performs the worst of all the mixes, as expected. All the parameters are significantly higher than mixes with one and two types of fibers. One thing to note is the difference between the stress in the ring and the tensile strength seen in Figure 4.7 below. Although the rings did not crack fully, the graph suggests that cracking may occur within 91 days. The difference between the tensile strength and the stress is much less than mixes with fibers. This also corresponds to free shrinkage, which explains why mixes that shrink more induce higher tensile stress under restrained conditions.

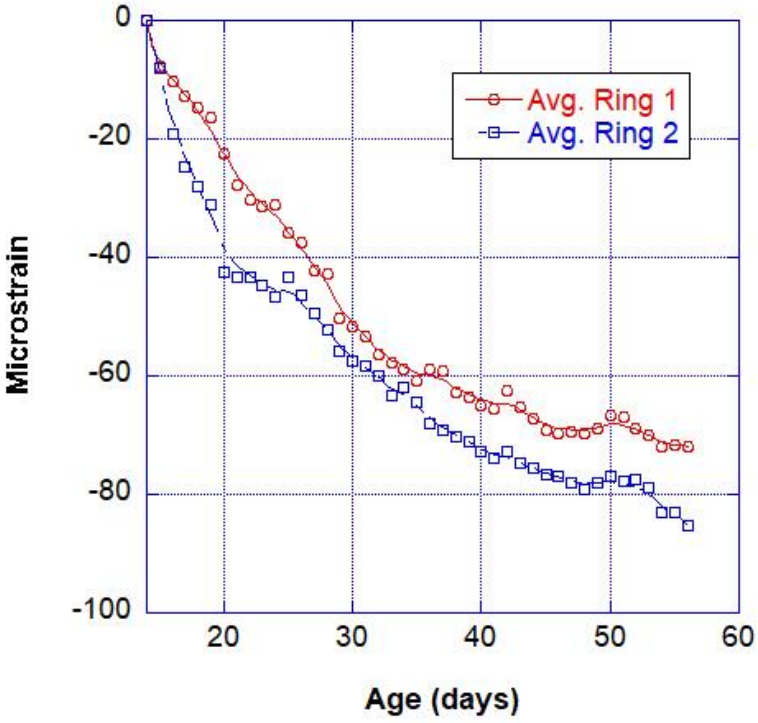

Figure 4.6 – $M^0N^0S^0$ FSG Data

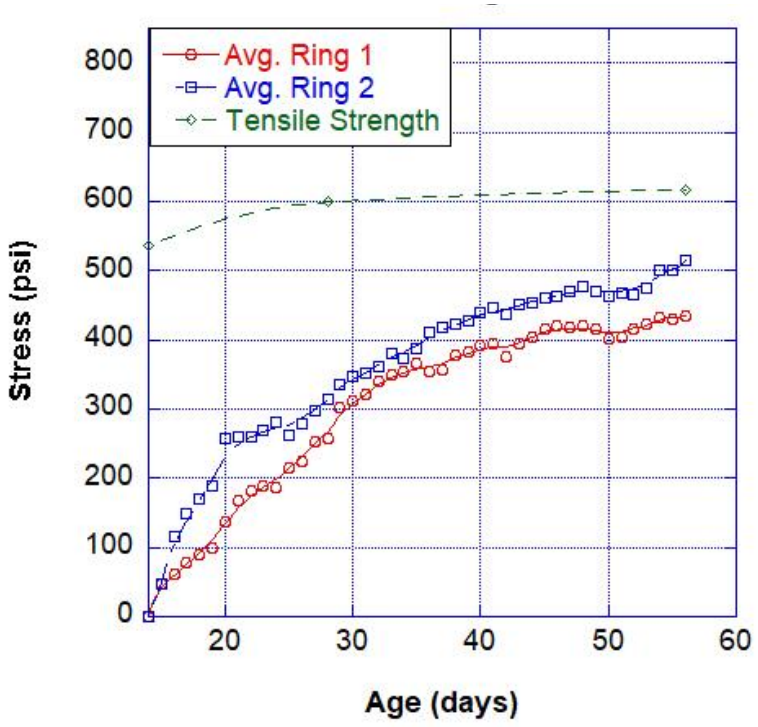

Figure 4.7 – $M^0N^0S^0$ Ring Stress

4.6.2 $M^0N^0S^{42}$

	Number of Cracks	Average Crack Width (in)	Maximum Crack Width (in)	Cracking Area (in^2)	Age of Cracking (days)
Ring 1	79	0.000594	0.00110	0.0834	TBD
Ring 2	77	0.000641	0.00106	0.0869	TBD
Average	**78**	**0.000618 σ = 0.000197**	**0.00110**	**0.0852**	**-**

Table 4.12 – $M^0N^0S^{42}$ 28-day crack mapping results

	Number of Cracks	Average Crack Width (in)	Maximum Crack Width (in)	Cracking Area (in^2)	Age of Cracking (days)
Ring 1	116	0.00633	0.00138	0.1202	None
Ring 2	110	0.000670	0.00110	0.1250	None
Average	**113**	**0.000652 σ = 0.000218**	**0.00138**	**0.1226**	**-**

Table 4.13 – $M^0N^0S^{42}$ 56-day crack mapping results

The addition of steel fibers at 42 lb/cy proved to be the optimal mix for just one type of fiber in terms of reducing number of cracks. This mix performs very similar in comparison to $M^5N^0S^0$ due to the fact that they both have equal fiber concentrations by volume. One thing to note is that the ring stress data did quite stabilize, suggesting that there is still stress accumulating in the concrete. However, the stress is still very well beneath the splitting tensile strength and does not show signs of macro-cracking. The FSG data and ring stress can be seen in Figure 4.8 and Figure 4.9 respectively.

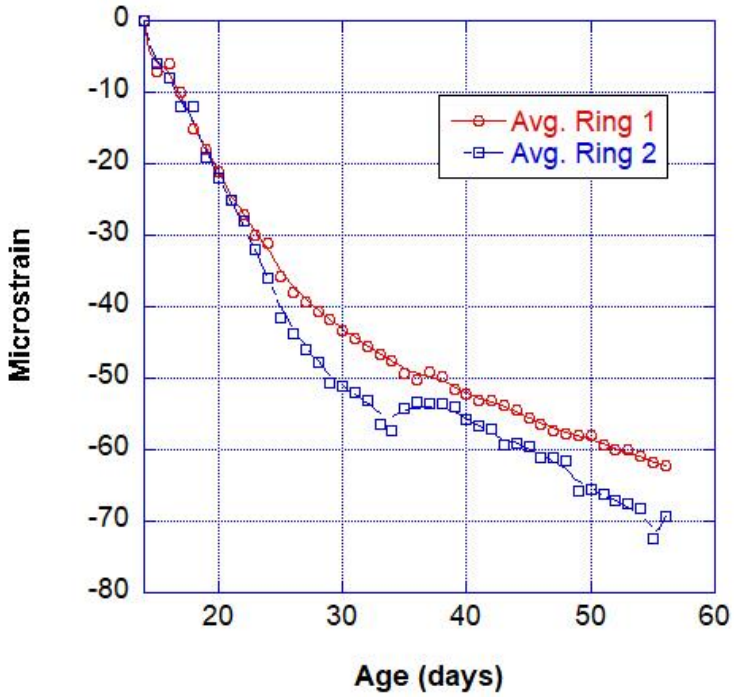

Figure 4.8 – $M^0N^0S^{42}$ FSG Data

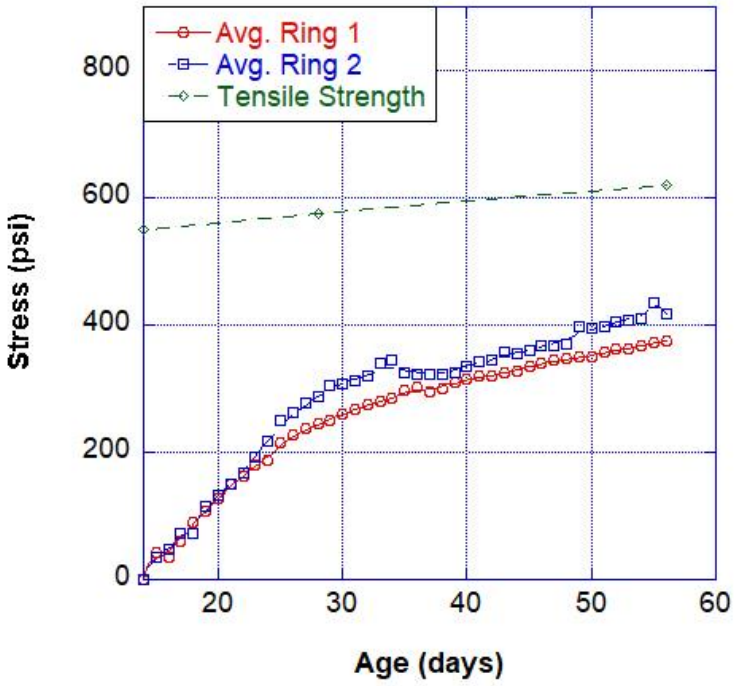

Figure 4.9 – $M^0N^0S^{42}$ Ring Stress

4.6.3 $M^5N^0S^0$

	Number of Cracks	Average Crack Width (in)	Maximum Crack Width (in)	Cracking Area (in^2)	Age of Cracking (days)
Ring 1	83	0.000624	0.00110	0.0871	TBD
Ring 2	79	0.000579	0.00118	0.0813	TBD
Average	**81**	**0.000602 σ = 0.000170**	**0.00118**	**0.0842**	**-**

Table 4.14 – $M^5N^0S^0$ 28-day crack mapping results

	Number of Cracks	Average Crack Width (in)	Maximum Crack Width (in)	Cracking Area (in^2)	Age of Cracking (days)
Ring 1	116	0.000670	0.00122	0.1273	None
Ring 2	117	0.000618	0.00126	0.1153	None
Average	**117**	**0.000644 σ = 0.000201**	**0.00126**	**0.1213**	**-**

Table 4.15 – $M^5N^0S^0$ 56-day crack mapping results

This mix is critical as it provides a datum to compare with the hybrids. The number of cracks remains low, reducing it by 32.5% in comparison to $M^0N^0S^0$ at 28 days. This indicates that macro fibers have a tendency to reduce the number of micro cracks in a mix. The average crack width is 7.8% less than $M^0N^0S^0$, in which reinforcing this mix with another fiber may improve this value. Overall, this mix performs very well, but improvements can most definitely be made. The FSG data shown in Figure 4.10 for ring 1 had some minor defects, but the overall trend can be seen by looking at both rings.

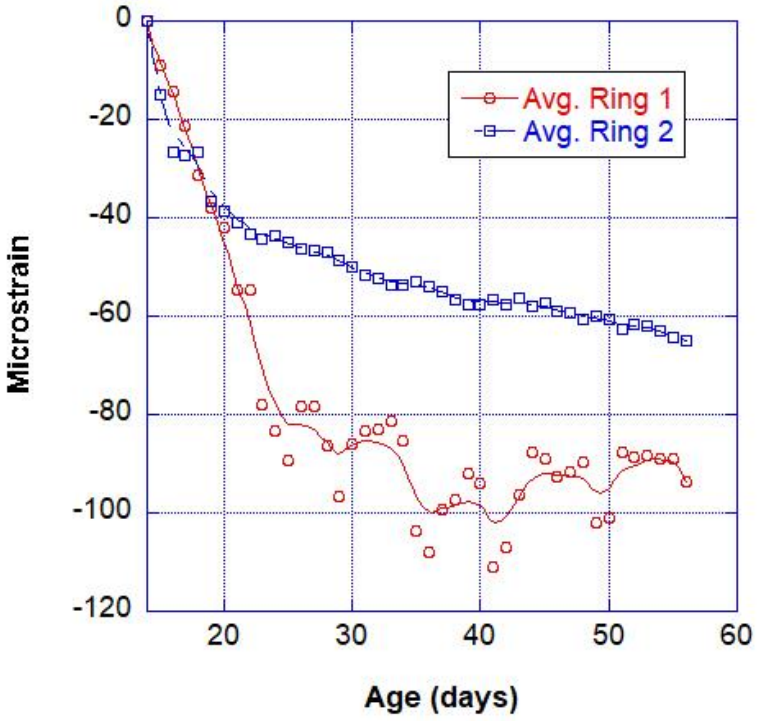

Figure 4.10 – $M^5N^0S^0$ 28-day crack mapping results

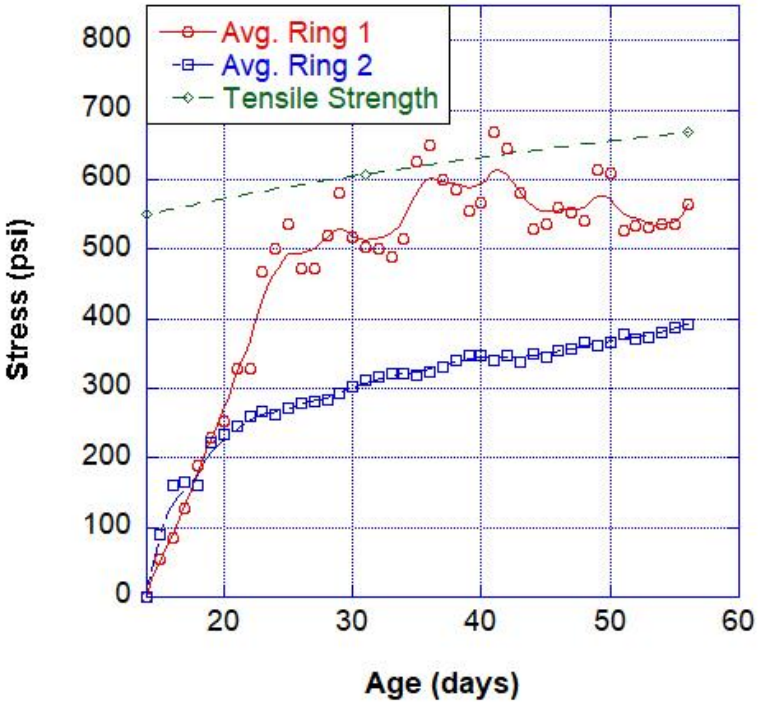

Figure 4.11 – $M^5N^0S^0$ 28-day crack mapping results

4.6.4 $M^{2.5}N^{0.5}S^{0}$

	Number of Cracks	Average Crack Width (in)	Maximum Crack Width (in)	Cracking Area (in^2)	Age of Cracking (days)
Ring 1	83	0.000578	0.00098	0.0920	TBD
Ring 2	84	0.000585	0.00110	0.0896	TBD
Average	**84**	**0.000582 σ = 0.000160**	**0.00110**	**0.0908**	**-**

Table 4.16 – $M^{2.5}N^{0.5}S^{0}$ 28-day crack mapping results

	Number of Cracks	Average Crack Width (in)	Maximum Crack Width (in)	Cracking Area (in^2)	Age of Cracking (days)
Ring 1	124	0.000668	0.00157	0.1361	None
Ring 2	127	0.000677	0.00126	0.1356	None
Average	**126**	**0.000673 σ = 0.000220**	**0.00157**	**0.1359**	**-**

Table 4.17 – $M^{2.5}N^{0.5}S^{0}$ 56-day crack mapping results

This mix performs relatively well despite having a low fiber content by volume. At 28 days, the number of cracks are significantly less than the control mix. However, at 56 days, the number of cracks increase appreciably and the cracks get much wider. Both of these may be explained by the low dose of fibers totaling at 0.19% by volume. The micro fibers tend to decrease crack width initially, but because the dose of macro fibers is low, the cracks got much wider between 28-56 days. The steel strain data and stress in the concrete can be seen in Figures 12 and 13 respectively. The large gap between the tensile strength and the stress in the concrete implies that cracking of the ring may never occur.

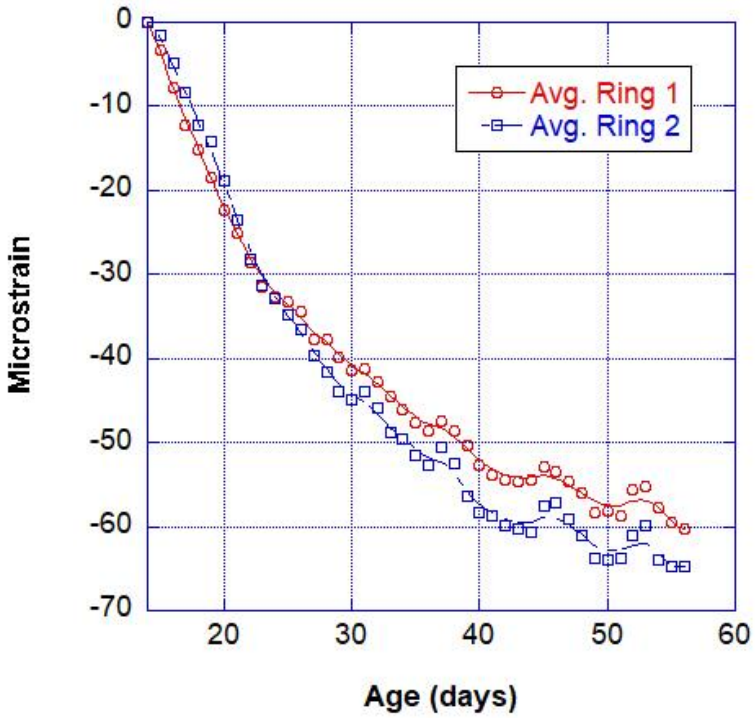

Figure 4.12 – $M^{2.5}N^{0.5}S^{0}$ FSG Data

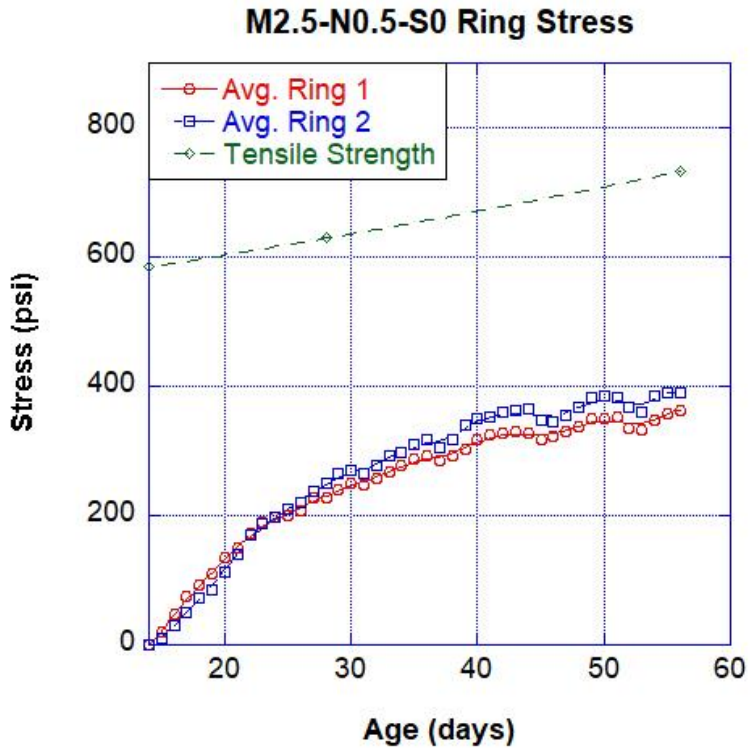

Figure 4.13 – $M^{2.5}N^{0.5}S^{0}$ Ring Stress

4.6.5 $M^5N^{0.5}S^0$

	Number of Cracks	Average Crack Width (in)	Maximum Crack Width (in)	Cracking Area (in^2)	Age of Cracking (days)
Ring 1	74	0.000589	0.00126	0.0786	TBD
Ring 2	79	0.000609	0.00102	0.0814	TBD
Average	**77**	**0.000599 σ = 0.000183**	**0.00126**	**0.0800**	**-**

Table 4.18 – $M^5N^{0.5}S^0$ 28-day crack mapping results

	Number of Cracks	Average Crack Width (in)	Maximum Crack Width (in)	Cracking Area (in^2)	Age of Cracking (days)
Ring 1	98	0.000624	0.00126	0.0999	None
Ring 2	101	0.000651	0.00122	0.1046	None
Average	**100**	**0.000638 σ = 0.000206**	**0.00126**	**0.1023**	**-**

Table 4.19 – $M^5N^{0.5}S^0$ 56-day crack mapping results

This mix performs significantly better than $M^{2.5}N^{0.5}S^0$ in almost every parameter, mainly due to the increased dose of macro fibers. At 56 days, the number of cracks in comparison to $M^5N^0S^0$ is reduced by 14.5%, suggesting that the increased amount of total fibers has some influence on total number of cracks. This also may be attributed to the synergistic effect created when macro and micro fibers are combined. This mix performs the best in terms of cracking area. One thing to also note is that the maximum crack width did not get any bigger between 28 and 56 days. It is predicted that the hybrid fibers prevented this crack growth. In addition, this mix had the smallest average crack width found in this study at 56 days. The FSG data and ring stress can be seen in Figures 4.14 and 4.15.

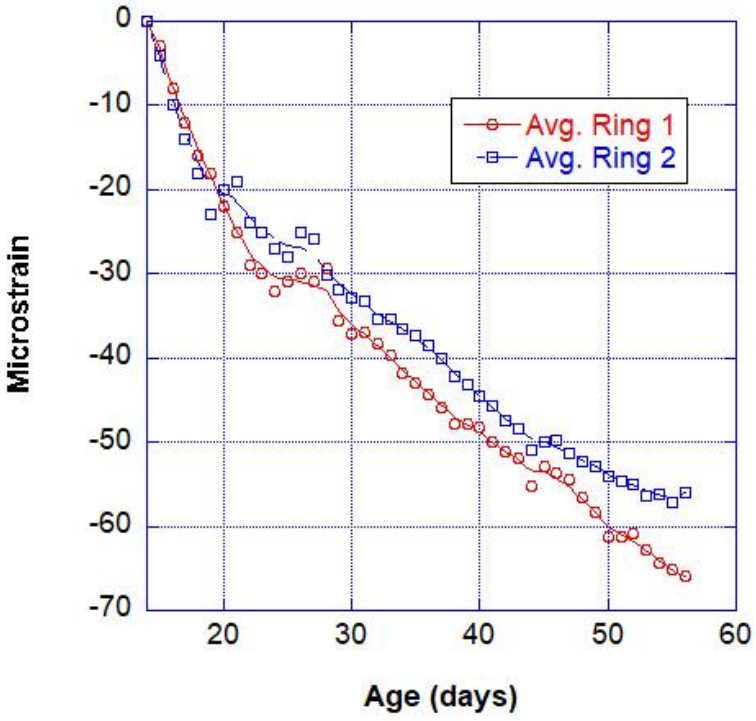

Figure 4.14 – $M^5N^{0.5}S^0$ FSG Data

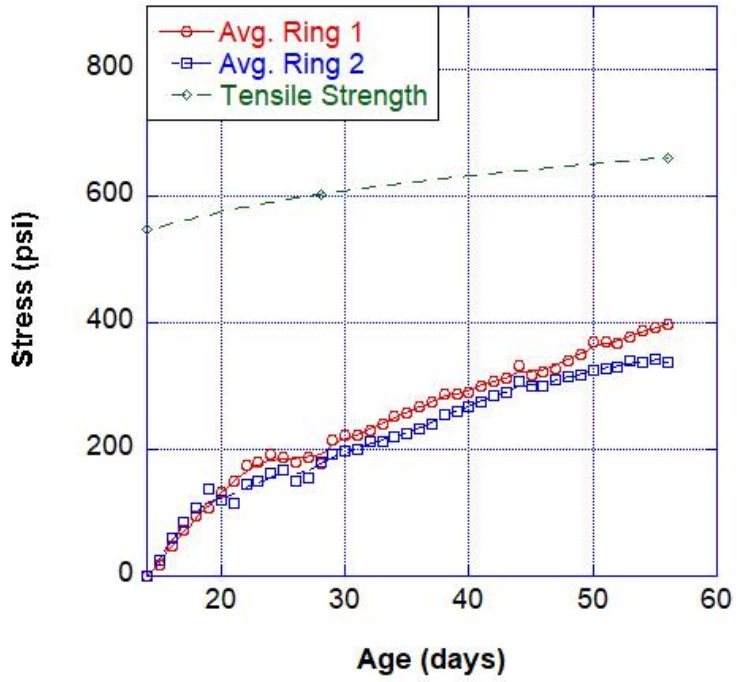

Figure 4.15 – $M^5N^{0.5}S^0$ Ring Stress

4.6.6 $M^0N^{0.5}S^{12.5}$

	Number of Cracks	Average Crack Width (in)	Maximum Crack Width (in)	Cracking Area (in^2)	Age of Cracking (days)
Ring 1	89	0.000559	0.00106	0.0911	TBD
Ring 2	91	0.000568	0.00114	0.0927	TBD
Average	**90**	**0.000564 σ = 0.000158**	**0.00114**	**0.0919**	**-**

Table 4.20 – $M^0N^{0.5}S^{12.5}$ 28-day crack mapping results

	Number of Cracks	Average Crack Width (in)	Maximum Crack Width (in)	Cracking Area (in^2)	Age of Cracking (days)
Ring 1	113	0.000707	0.00138	0.1342	None
Ring 2	123	0.000648	0.00138	0.1267	None
Average	**118**	**0.000678 σ = 0.000223**	**0.00138**	**0.1305**	**-**

Table 4.21 – $M^0N^{0.5}S^{12.5}$ 56-day crack mapping results

From inspection, one can identify several pros and cons about this mix. Similar to $M^{2.5}N^{0.5}S^0$, the initial average crack width is low, possibly due to the presence of micro fibers. The number of cracks is initially higher than $M^{2.5}N^{0.5}S^0$, but at 56 days, the total number of cracks becomes less. This mix performs well in terms of maximum crack width, providing 26.9% decrease in comparison to the mix without any fibers. Cracking area is drastically reduced from the control mix, but remains similar to all mixes with fibers. The FSG data and the ring stress is presented in Figures 4.16 and 4.17 below. Similar to $M^{2.5}N^{0.5}S^0$, the stress in the concrete is significantly less than the tensile strength, suggesting that cracking may never occur.

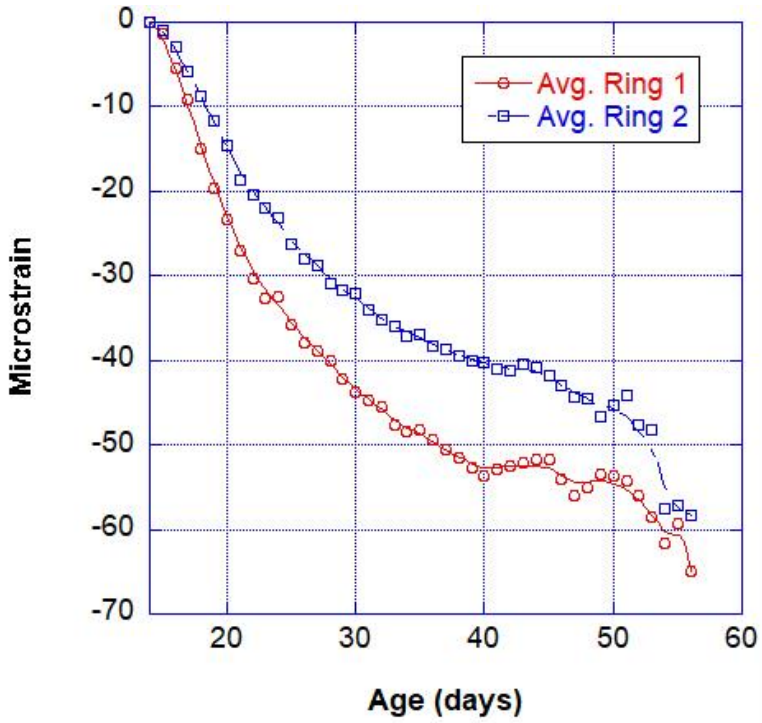

Figure 4.16 – $M^0N^{0.5}S^{12.5}$ FSG Data

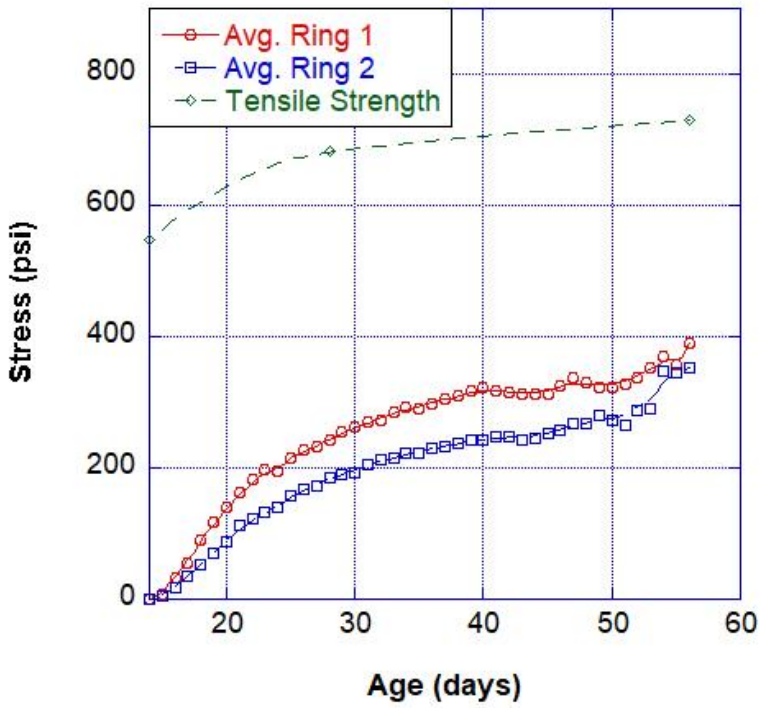

Figure 4.17 – $M^0N^{0.5}S^{12.5}$ Ring Stress

4.6.7 $M^5N^0S^5$

	Number of Cracks	Average Crack Width (in)	Maximum Crack Width (in)	Cracking Area (in^2)	Age of Cracking (days)
Ring 1	83	0.000613	0.00122	0.0817	TBD
Ring 2	72	0.000631	0.00126	0.0896	TBD
Average	**78**	**0.000622 σ = 0.000190**	**0.00126**	**0.0857**	**-**

Table 4.22 – $M^5N^0S^5$ 28-day crack mapping results

	Number of Cracks	Average Crack Width (in)	Maximum Crack Width (in)	Cracking Area (in^2)	Age of Cracking (days)
Ring 1	111	0.000644	0.00133	0.1054	None
Ring 2	97	0.000705	0.00134	0.1149	None
Average	**104**	**0.000685 σ = 0.000240**	**0.00134**	**0.1102**	**-**

Table 4.23 – $M^5N^0S^5$ 56-day crack mapping results

This mix performs well in terms of number of cracks and cracking area, but does not perform well in average and maximum crack width. The addition of steel fibers into the matrix reduced the number of cracks and overall severity of the cracks experienced on the surface, but the average crack width was not improved. Average crack width increased by 5.1% and 6.3% in comparison to $M^0N^0S^{42}$ and $M^5N^0S^0$ respectively. This increase is very minor, but this further provides evidence that micro fibers reduce average crack width. The FSG data and ring stress can be seen below in Figures 4.18 and 4.19.

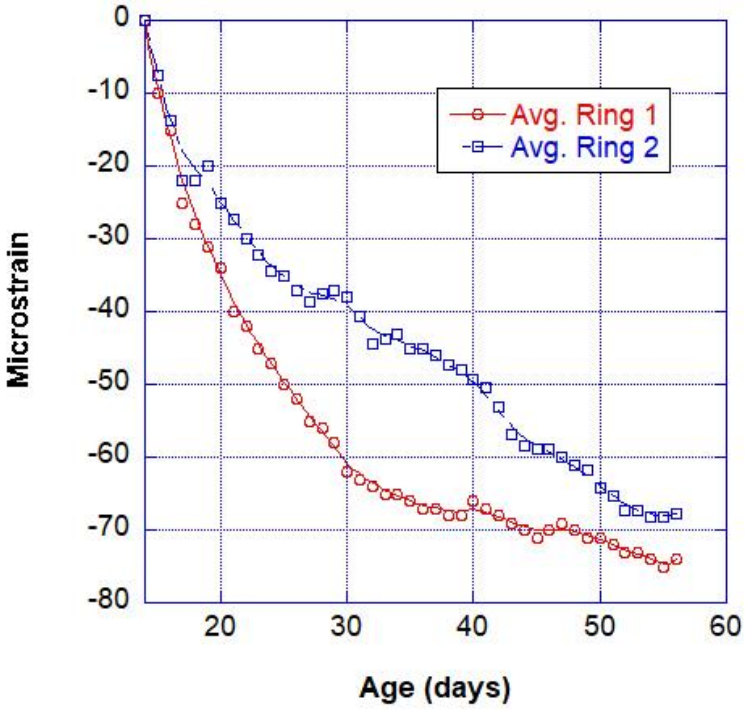

Figure 4.18 – $M^5N^0S^5$ FSG Data

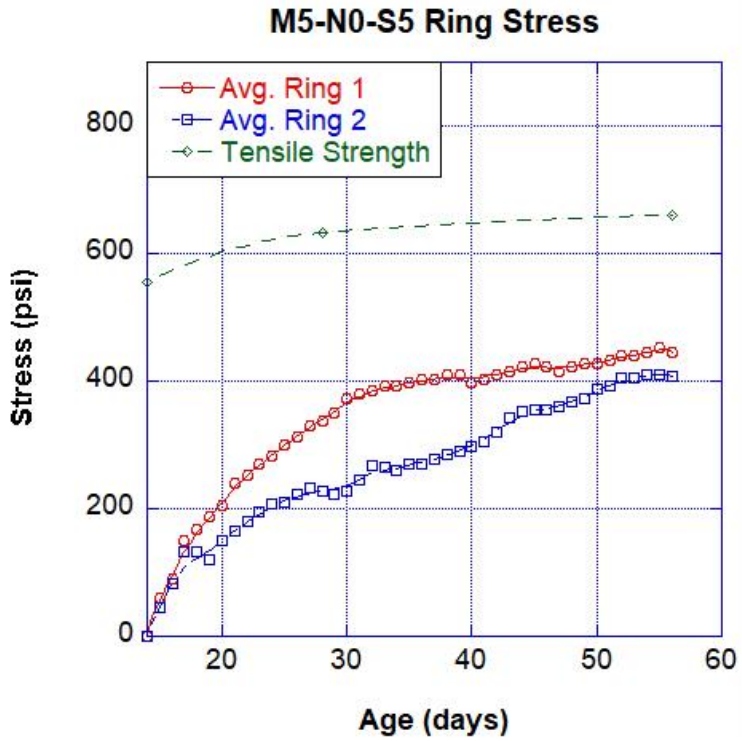

Figure 4.19 – $M^5N^0S^5$ Ring Stress

4.6.8 $M^5N^0S^7$

	Number of Cracks	Average Crack Width (in)	Maximum Crack Width (in)	Cracking Area (in^2)	Age of Cracking (days)
Ring 1	72	0.000587	0.00102	0.0845	TBD
Ring 2	68	0.000602	0.00102	0.0780	TBD
Average	**70**	**0.000595 σ = 0.000165**	**0.00102**	**0.0813**	**-**

Table 4.24 – $M^5N^0S^7$ 28-day crack mapping results

	Number of Cracks	Average Crack Width (in)	Maximum Crack Width (in)	Cracking Area (in^2)	Age of Cracking (days)
Ring 1	100	0.000672	0.00130	0.1142	None
Ring 2	94	0.000690	0.00126	0.1073	None
Average	**97**	**0.000681 σ = 0.000213**	**0.00130**	**0.1108**	**-**

Table 4.25 – $M^5N^0S^7$ 56-day crack mapping results

This mix is very similar to $M^5N^0S^5$ but performs slightly better as expected. At 56 days, there is 6.7% less cracks than $M^5N^0S^5$, further suggesting that macro and steel fibers have influence on the total number of cracks. When combined together, they reduce the number of cracks by 30.7%, 14.2% and 16.7% in comparison to $M^0N^0S^0$, $M^0N^0S^{42}$, and $M^5N^0S^0$ respectively. In addition, this mix had the least number of cracks in this experiment. The FSG data and ring stress can be seen in Figures 4.20 and 4.21 below.

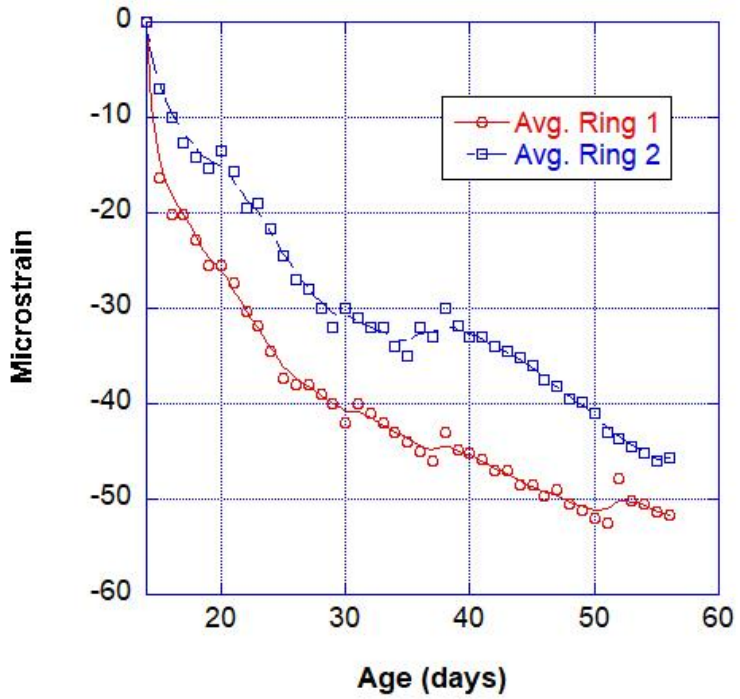

Figure 4.20 – $M^5N^0S^7$ FSG Data

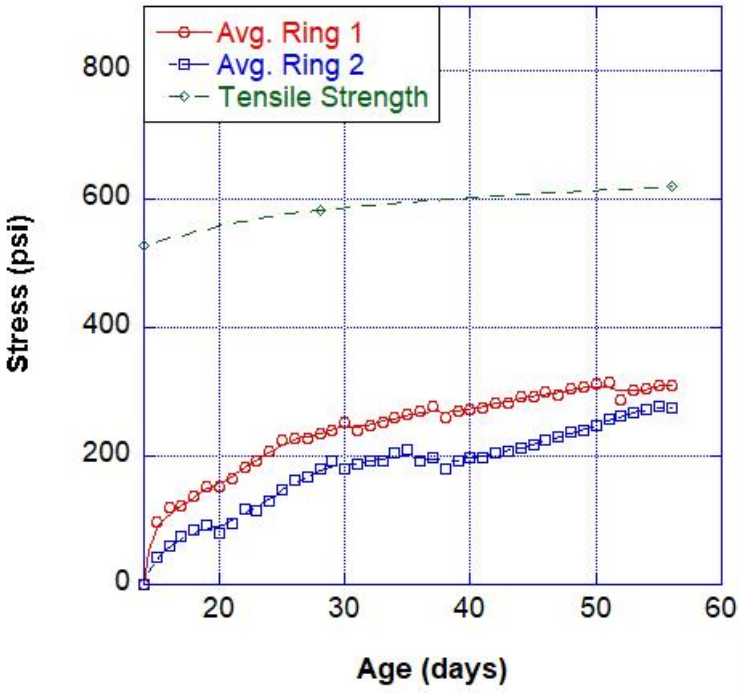

Figure 4.21 – $M^5N^0S^7$ Ring Stress

4.7 Crack Mapping Comparison

The main parameters of each mix that will be compared are number of cracks, average crack width, maximum crack width, and crack area. Each mix will be compared to the three control mixes: $M^0N^0S^0$, $M^5N^0S^0$, and $M^0N^0S^{42}$. One of the main objectives of this research is to improve the cracking frequency of $M^5N^0S^0$ by supplementing this mix with a secondary fiber. The comparison are as follows.

4.7.1 Number of Cracks

Age	$M^0N^0S^0$		$M^0N^0S^{42}$		$M^5N^0S^0$		$M^{2.5}N^{0.5}S^0$		$M^5N^{0.5}S^0$		$M^0N^{0.5}S^{12.5}$		$M^5N^0S^5$		$M^5N^0S^7$	
28	120	-	78	-34.7%	81	-32.2%	84	-30.1%	77	-36.0%	90	-24.7%	78	-35.1%	70	-41.4%
		53.2%		-		3.8%		7.1%		-1.9%		15.4%		-0.6%		-10.3%
		47.5%		-3.7%		-		3.1%		-5.6%		11.1%		-4.3%		-13.6%
56	140	-	113	-19.3%	117	-16.8%	126	-10.4%	100	-28.9%	118	-15.7%	104	-25.7%	97	-30.7%
		23.9%		-		3.1%		11.1%		-11.9%		4.4%		-8.0%		-14.2%
		20.2%		-3.0%		-		7.7%		-14.6%		1.3%		-10.7%		-16.7%

Table 4.26 – Number of cracks comparison

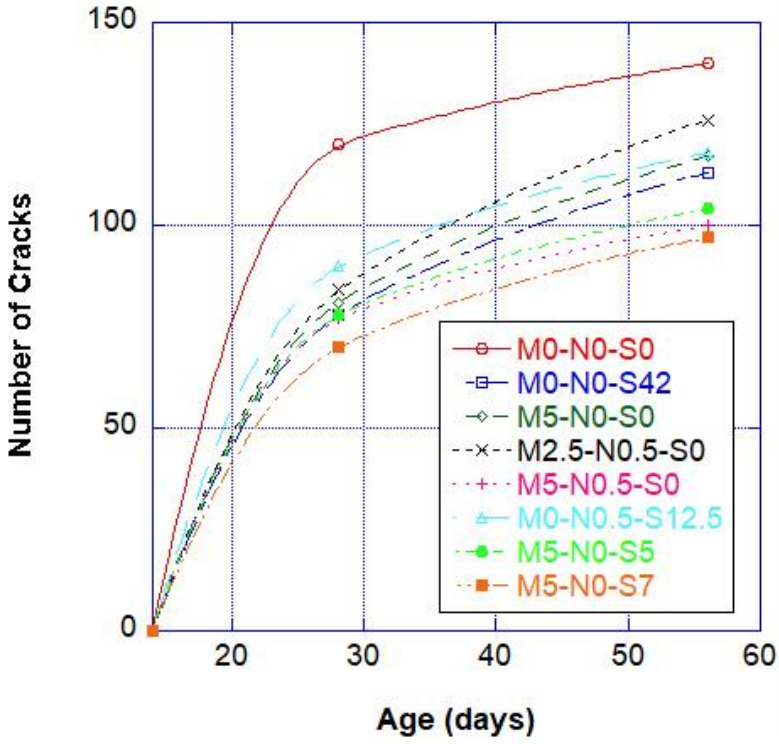

Figure 4.22 – Number of cracks vs. time

By inspection of Table 4.26, a few conclusions can be made. First, $M^0N^0S^0$ performs the worst, as expected. In addition, at the same dose by volume, steel fibers are slightly more effective at reducing the number of cracks in comparison to macro fibers, by 3% at 56 days. $M^5N^0S^7$ provides the least number of cracks at 56 days, reducing the number of cracks by 14.2% and 16.7% in comparison to $M^0N^0S^{42}$ and $M^5N^0S^0$ respectively. $M^5N^{0.5}S^0$ is next in terms of performance, reducing the number of cracks by 11.9% and 14.6% in comparison to $M^0N^0S^{42}$ and $M^5N^0S^0$ respectively. To expand, $M^{2.5}N^{0.5}S^0$ and $M^0N^{0.5}S^{12.5}$ did not perform better than the fiber control mixes at 56 days, possibly due to a lower fiber concentration by volume. In conclusion, hybrid combinations of macro & steel fibers, and macro & micro fibers proved to be better than the control mixes in regards to reducing the number of cracks.

4.7.2 Average Crack Width

Age	$M^0N^0S^0$		$M^0N^0S^{42}$		$M^5N^0S^0$		$M^{2.5}N^{0.5}S^0$		$M^5N^{0.5}S^0$		$M^0N^{0.5}S^{12.5}$		$M^5N^0S^5$		$M^5N^0S^7$	
28	0.000653	-	0.000618	-5.4%	0.000602	-7.9%	0.000582	-10.9%	0.000599	-8.3%	0.000564	-13.7%	0.000622	-4.7%	0.000595	-9.0%
		5.7%		-		-2.6%		-5.8%		-3.0%		-8.7%		0.7%		-3.7%
		8.6%		2.7%		-		-3.3%		-0.4%		-6.3%		3.4%		-1.2%
56	0.000708	-	0.000652	-7.9%	0.000644	-9.0%	0.000673	-4.9%	0.000638	-9.9%	0.000678	-4.2%	0.000685	-3.3%	0.000681	-3.7%
		8.6%		-		-1.2%		3.2%		-2.1%		4.0%		5.1%		4.5%
		9.9%		1.2%		-		4.4%		-1.0%		5.2%		6.3%		5.7%

Table 4.27 – Average crack width (in) comparison

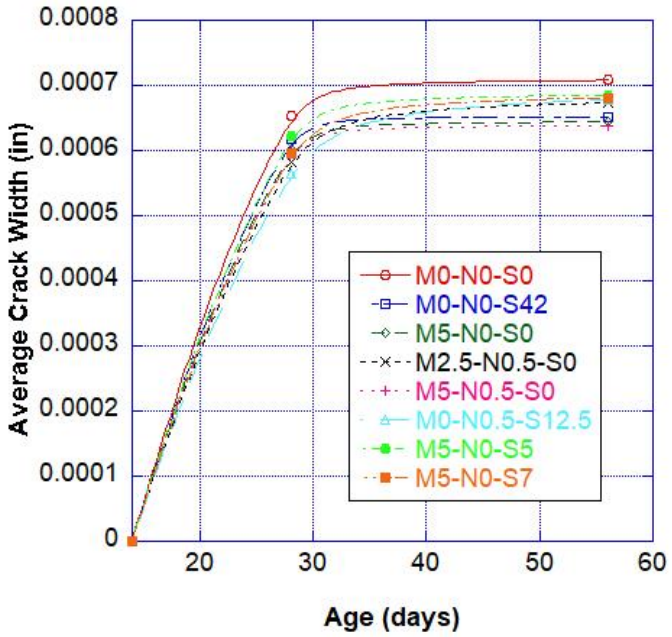

Figure 4.23 – Average crack width vs. time

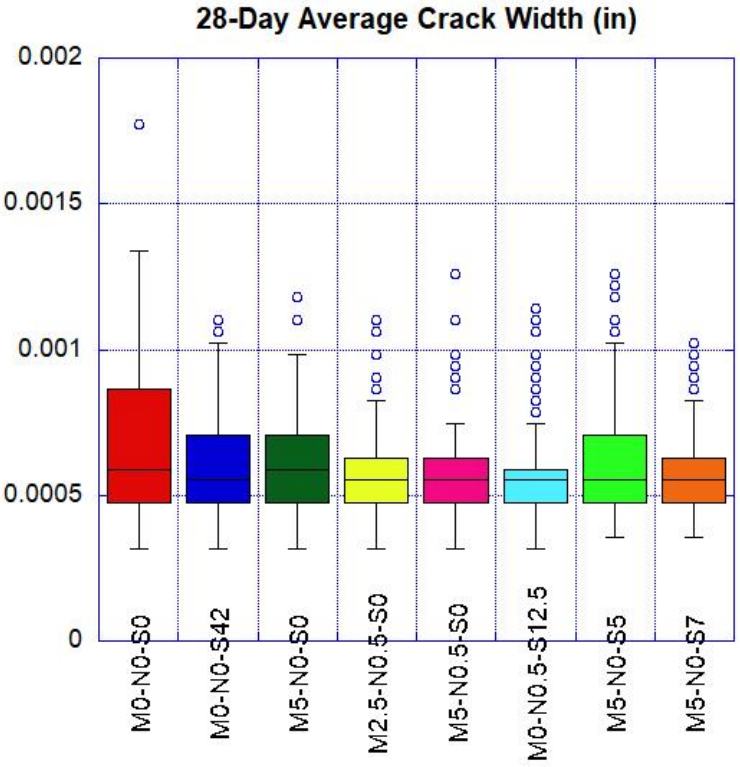

Figure 4.24 – 28-day average crack width statistical comparison

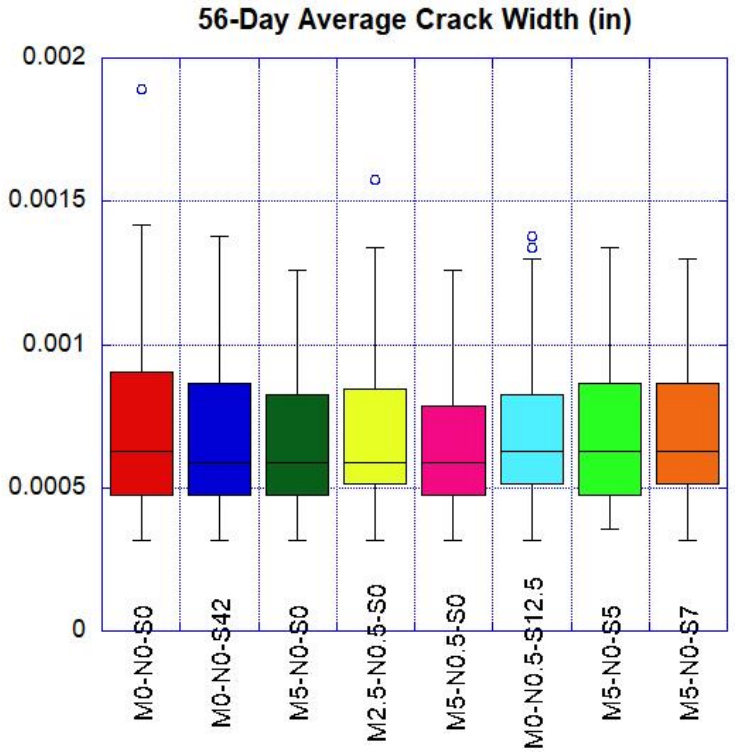

Figure 4.25 – 56-day average crack width statistical comparison

Overall, the average crack width is the parameter that is least affected with the addition of any fibers. This is estimated due to the fact that measurements are taken of microcracks. It is predicted that fibers will improve macrocrack width much more than microcracks. Firstly, the mix that performs the best at 56 days is $M^5N^{0.5}S^0$. The average crack width is reduced by 2.1% and 1.0% in comparison to $M^0N^0S^{42}$ and $M^5N^0S^0$ respectively. This mix also reduces crack width by 9.9% in comparison to the control mix without any fibers. One thing to note is that both $M^5N^0S^5$ and $M^5N^0S^7$ have slightly higher average crack width than both control mixes, which confirms the fact that steel and macro fibers have little effect on microcrack width. Perhaps if a macrocrack were to occur, the crack width could be reduced. In conclusion, $M^5N^{0.5}S^0$ performs the best in terms of average crack width, suggesting that micro fibers help control crack width. This can be seen visually in Figures 4.24 and 4.25.

4.7.3 Maximum Crack Width

Age	$M^0N^0S^0$		$M^0N^0S^{42}$		$M^5N^0S^0$		$M^{2.5}N^{0.5}S^0$		$M^5N^{0.5}S^0$		$M^0N^{0.5}S^{12.5}$		$M^5N^0S^5$		$M^5N^0S^7$	
28	0.00177	-	0.00110	-37.9%	0.00118	-33.3%	0.00110	-37.9%	0.00126	-28.8%	0.00114	-35.6%	0.00126	-28.8%	0.00102	-42.4%
		60.9%		-		7.3%		0.0%		14.5%		3.6%		14.5%		-7.3%
		50.0%		-6.8%		-		-6.8%		6.8%		-3.4%		6.8%		-13.6%
56	0.00189	-	0.00138	-27.0%	0.00126	-33.3%	0.00157	-16.9%	0.00126	-33.3%	0.00138	-27.0%	0.00134	-29.1%	0.00130	-31.2%
		37.0%		-		-8.7%		13.8%		-8.7%		0.0%		-2.9%		-5.8%
		50.0%		9.5%		-		24.6%		0.0%		9.5%		6.3%		3.2%

Table 4.28 – Maximum crack width (in) comparison

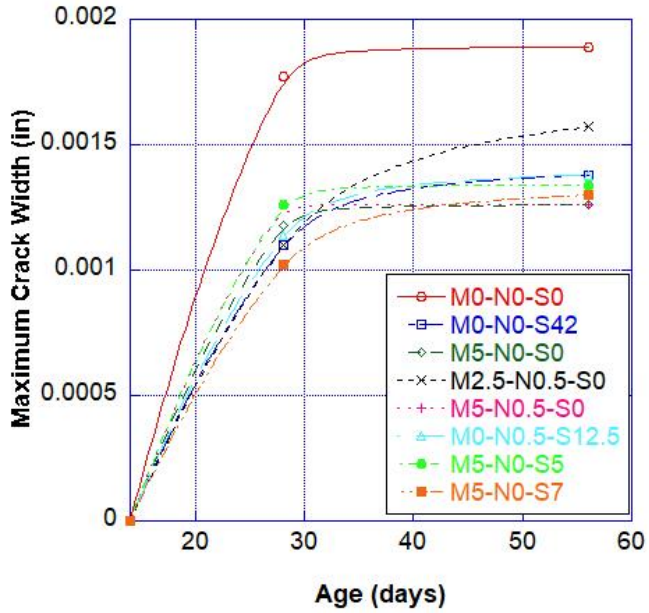

Figure 4.26 – Maximum crack width vs. time

The maximum crack width results are very similar to the average crack width results. $M^5N^0S^0$ and $M^5N^{0.5}S^0$ both perform the best at 56 days, improving maximum crack width by 33.3% in comparison to $M^0N^0S^0$. In addition, $M^5N^0S^5$ and $M^5N^0S^7$ outperform $M^0N^0S^{42}$ by 2.9% and 5.8% respectively. However, they display a larger maximum crack width than $M^5N^0S^0$. As stated earlier, this may be due to the fact that measurements are being taken of microcracks instead of macrocracks. It is predicted that if macrocracks were to occur, the behavior of these mixes would improve in comparison to the control mixes. In conclusion, hybrid fibers do not improve maximum crack width of microcracks, but more investigation is required to see their impact on macrocracks.

4.7.4 Cracking Area

Age	$M^0N^0S^0$		$M^0N^0S^{42}$		$M^5N^0S^0$		$M^{2.5}N^{0.5}S^0$		$M^5N^{0.5}S^0$		$M^0N^{0.5}S^{12.5}$		$M^5N^0S^5$		$M^5N^0S^7$	
28	0.1402	-	0.0852	-39.2%	0.0842	-39.9%	0.0908	-35.2%	0.0800	-42.9%	0.0919	-34.4%	0.0857	-38.9%	0.0813	-42.0%
		64.6%		-		-1.1%		6.6%		-6.0%		7.9%		0.6%		-4.6%
		66.4%		1.1%		-		7.8%		-5.0%		9.1%		1.7%		-3.5%
56	0.1681	-	0.1226	-27.1%	0.1213	-27.8%	0.1359	-19.2%	0.1023	-39.2%	0.1305	-22.4%	0.1102	-34.5%	0.1108	-34.1%
		37.1%		-		-1.1%		10.8%		-16.6%		6.4%		-10.2%		-9.7%
		38.6%		1.1%		-		12.0%		-15.7%		7.5%		-9.2%		-8.7%

Table 4.29 – Cracking area (in^2) comparison

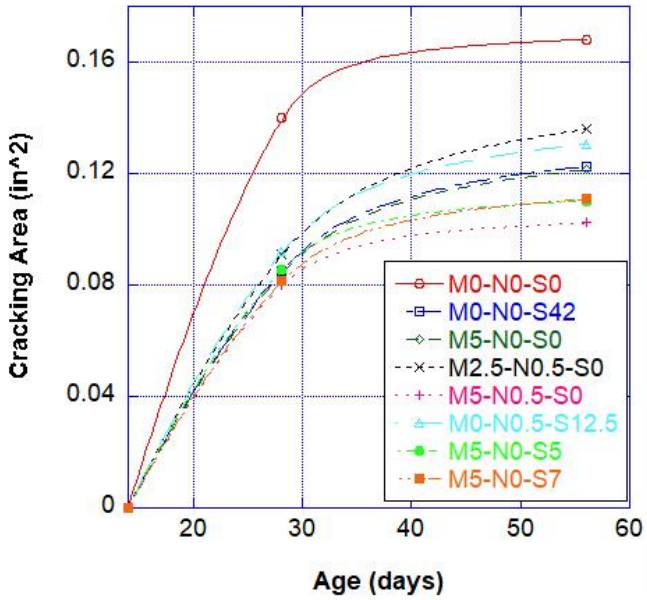

Figure 4.27 – Cracking area vs. time

Cracking area is one parameter that is significantly improved with the implementation of any fibers. All of the hybrids outperform the control fiber mixes with the exception of $M^{2.5}N^{0.5}S^{0}$ and $M^{0}N^{0.5}S^{12.5}$. This is due to their lower fiber dose by volume. $M^{5}N^{0.5}S^{0}$ outperforms $M^{5}N^{0}S^{0}$ and $M^{0}N^{0}S^{42}$ by 16.6% and 15.7% respectively. In addition, $M^{5}N^{0}S^{5}$ performs very similarly to $M^{5}N^{0}S^{7}$, as expected. They both reduce the cracking area in comparison to $M^{0}N^{0}S^{42}$ by 10.2% and 9.7% respectively. They also reduce the cracking area in comparison to $M^{5}N^{0}S^{0}$ by 9.2% and 8.7% respectively. In conclusion, the hybrid fibers containing macro and micro fibers performs the best in regards to cracking area.

4.7.5 Average Crack Length

Age	$M^0N^0S^0$		$M^0N^0S^{42}$		$M^5N^0S^0$		$M^{2.5}N^{0.5}S^0$		$M^5N^{0.5}S^0$		$M^0N^{0.5}S^{12.5}$		$M^5N^0S^5$		$M^5N^0S^7$	
28	1.6751	-	1.7406	3.9%	1.6466	-1.7%	1.8162	8.4%	1.7503	4.5%	1.8323	9.4%	1.7314	3.4%	2.0291	21.1%
		-3.8%		-		-5.4%		4.3%		0.6%		5.3%		-0.5%		16.6%
		1.7%		5.7%		-		10.3%		6.3%		11.3%		5.2%		23.2%
56	1.5436	-	1.4490	-6.1%	1.4533	-5.8%	1.4697	-4.8%	1.4926	-3.3%	1.5130	-2.0%	1.4173	-8.2%	1.5915	3.1%
		6.5%		-		0.3%		1.4%		3.0%		4.4%		-2.2%		9.8%
		6.2%		-0.3%		-		1.1%		2.7%		4.1%		-2.5%		9.5%

Table 4.30 – Average crack length comparison (in)

The average crack length is one parameter that does not have display drastic benefit by fiber implementation. This could be attributed to the fact that exact measurements are not taken of the crack length, rather it is being visually estimated by the crack mapper. It is important to keep this in mind when analyzing this parameter. At 56 days, it can be concluded that all fiber mixes have an average crack length that is less than the control mix without fibers. The only exception is $M^5N^0S^7$, which could be a result of the steel rings providing uneven restraint. By inspection of Table 4.30, it can be concluded that there is no benefit to hybrid implementation in reducing the average crack length. As stated earlier, microcrack analysis is being done and this test cannot predict what will occur when macrocracks occur. Therefore, there is a need to modify this test in order to further investigate macrocrack width and length.

4.8 Mix Ranking

In order to evaluate each of the mixes with a combination of the most parameters, a grading scale will be created. This scale will give the ability to evaluate and grade each mix. The scale and grading of each mix can be seen in Table 4.31 and Table 4.32.

Weight	Points/Range										
Compressive Strength @56d											
6%	0	10	20	30	40	50	60	70	80	90	100
	<8100	8100-8200	8200-8300	8300-8400	8400-8500	8500-8600	8600-8700	8700-8800	8800-8900	8900-9000	>9000
Tensile Strength @56d											
10%	0	10	20	30	40	50	60	70	80	90	100
	<590	590-600	600-610	610-620	620-640	640-650	650-680	680-720	730-740	740-750	>750
Modulus of Elasticity @56d											
2%	0	20	40	60	80	90	100	90	80	70	60
	<4100	4100-4200	4200-4300	4300-4400	4400-4500	4500-4600	4700-4900	4900-5000	4700-5100	5100-5200	>5300
Modulus of Rupture @ 28d											
10%	0	10	20	40	50	60	70	80	90	100	80
	<590	590-500	600-610	610-620	620-635	635-650	650-660	660-680	680-700	700-750	>750
Chloride Permeability@56d											
5%	100	90	80	70	60	50	40	30	20	10	0
	<600	600-700	700-800	800-1200	1200-1500	1500-1800	1800-2000	2000-2500	2500-3000	3000-3500	>3500
Workability (in)											
2%	0	10	20	40	60	80	100	80	60	40	30
	<1	1-2	2-3	3-4	4-5	5-6	6-7	7-8	8-9	10-11	11-12
Number of Cracks @56d											
15%	100	90	80	70	60	50	40	30	20	10	0
	<100	100-105	105-115	115-120	120-125	125-130	130-140	140-150	150-160	160-170	>170
Average Crack Width @56d											
10%	0	10	20	30	40	50	60	70	80	90	100
						>0.000700	0.000680-0.000700	0.000660-0.000680	0.000660-640	0.000640-0.000620	<0.000620
Maximim Crack Width @56d											
10%							40	60	70	80	100
							0.0018-0.0020	0.0016-0.0018	0.0014-0.0016	0.0012-0.14	<0.0012
Crack Area @56d											
15%							60	70	80	90	100
							0.1600-0.1700	0.1500-1600	0.1300-0.1500	0.1100-0.1300	0.1000-0.1100
Free Shrinkage @56d											
15%			20	30	40	50	60	70	80	90	100
	>300	280-290	270-280	260-270	250-260	240-250	230-240	220-230	200-220	<200	

Table 4.31 – Mix ranking weight & points

Mix Design	$M^0N^0S^0$	$M^0N^0S^{42}$	$M^5N^0S^0$	$M^{2.5}N^{0.5}S^0$	$M^5N^{0.5}S^0$	$M^0N^{0.5}S^{12.5}$	$M^5N^0S^5$	$M^5N^0S^7$
Compressive Strength @56d	8221	8838	8519	8041	8917	8333	9076	8559
Score	**1.2**	**4.8**	**3**	**0**	**5.4**	**1.8**	**6**	**3**
Tensile Strength @56d	617	619	668	732	673	661	661	619
Score	**3**	**3**	**6**	**8**	**6**	**6**	**6**	**3**
Modulus of Elasticity @56d	4607	4908	4553	4515	4577	4754	4632	4572
Score	**1.8**	**1.8**	**1.8**	**1.8**	**1.8**	**2**	**1.8**	**1.8**
Modulus of Rupture @56d	603	610	655	679	678	751	722	678
Score	**2**	**2**	**7**	**8**	**8**	**10**	**10**	**8**
Chloride Permeability @56d	771	1428	834	1088	790	1170	1753	1952
Score	**4**	**3**	**3.5**	**3.5**	**4**	**3.5**	**2.5**	**2**
Workability (in)	5	5.5	3.5	5	4	7	5.5	3.5
Score	**1.2**	**1.6**	**0.8**	**1.2**	**1.2**	**2**	**1.6**	**0.8**
Number of Cracks @56d	140	113	116.5	125.5	99.5	118	104	97
Score	**4.5**	**12**	**10.5**	**7.5**	**15**	**10.5**	**13.5**	**15**
Average Crack Width @56d	0.000708	0.000652	0.000644	0.000673	0.000638	0.0006775	0.000685	0.000681
Score	**5**	**8**	**8**	**7**	**9**	**7**	**6**	**6**
Maximum Crack Width @56d	0.00189	0.00138	0.00126	0.00157	0.00126	0.00138	0.00134	0.0013
Score	**4**	**8**	**8**	**7**	**8**	**8**	**8**	**8**
Crack Area @56d	0.1681	0.1226	0.1213	0.13585	0.10225	0.13045	0.11015	0.11075
Score	**9**	**13.5**	**13.5**	**12**	**15**	**12**	**13.5**	**13.5**
Free Shrinkage @56d	270	220	265	250	210	247.5	240	235
Score	**3**	**10.5**	**4.5**	**6**	**12**	**7.5**	**9**	**9**
Total	**38.7**	**68.2**	**66.6**	**62**	**85.4**	**70.3**	**77.9**	**70.1**

Table 4.32 – Mix ranking

Based on Table 4.32, a few conclusions can be made. It is clear that the control mix without fibers performs the worst. $M^5N^{0.5}S^0$ performs the best, suggesting that this mix may have strong potential in increasing restrained shrinkage cracking resistance.

$M^5N^0S^5$ also performs very well in comparison to the control fiber mixes. In conclusion, $M^5N^{0.5}S^0$ and $M^5N^0S^5$ are the best hybrids and outperform the control mixes significantly.

5. Conclusion

In conclusion, it is proven that hybrid fiber-reinforced high-performance concrete performs better than HPC reinforced with just one type of fiber. Various combinations of hybrids with different doses are deemed better than others. The test performed on each mix include fresh properties, compressive strength, splitting tensile strength, modulus of elasticity, modulus of rupture, surface resistivity, rapid chloride permeability, free shrinkage, and restrained shrinkage. The following summarizes the results of this experiment:

- Hybrid fiber-reinforced concrete has similar fresh properties in comparison to fiber-reinforced concrete. Slump is reduced, but air content was found to be unaffected in this experiment.
- All fiber-reinforced concrete mixes display higher compressive strength at early ages, possibly due to the fibers intercepting the microcracks as they occur. $M^{2.5}N^{0.5}S^{0}$ performs the best, increasing the 1-day compressive strength by 27.4%, 14.8%, and 5.1% in comparison to $M^{0}N^{0}S^{0}$, $M^{0}N^{0}S^{42}$, and $M^{0}N^{0}S^{42}$ respectively. As the specimens age, this increase becomes negligible. This suggests that macro fibers tend to increase early age compressive strength than other types of fibers.
- The modulus of elasticity is not significantly affected with the addition of any fibers, but steel fibers provide a slight increase of 6.5% in comparison to the control mix without any fibers.

- $M^{2.5}N^{0.5}S^{0}$ and $M^{5}N^{0.5}S^{0}$ both provide an increase of 18.3% and 8.7% respectively in tensile strength in comparison to $M^{5}N^{0}S^{0}$, suggesting that a hybrid combination of macro and micro fibers provide synergy in improving the tensile strength.
- Combinations of steel and micro fibers provided the best improvement for modulus of rupture, increasing the resistance by 14.5% in comparison to macro fibers alone.
- $M^{5}N^{0}S^{5}$ has a higher tensile strength and rupture modulus than $M^{5}N^{0}S^{7}$, suggesting that 5 lb per cubic yard of steel fibers is the right dose to reinforce as a hybrid fiber combination.
- Hybrid mixes displayed upwards to 15.7% increase in permeability versus mixes that had just one type of fiber. In addition, hybrids consisting of steel fibers higher than 0.32% by volume displayed a substantial increase in permeability.
- $M^{2.5}N^{0.5}S^{0}$ and $M^{5}N^{0.5}S^{0}$ reduce free shrinkage by 5.7% and 20.8% respectively in comparison to $M^{5}N^{0}S^{0}$. This may be attributed to the micro fibers reducing free shrinkage.
- $M^{5}N^{0}S^{7}$ provides the least number of cracks at 56 days, reducing the number of cracks by 14.2% and 16.7% in comparison to $M^{0}N^{0}S^{42}$ and $M^{5}N^{0}S^{0}$ respectively.
- The average crack width of $M^{5}N^{0.5}S^{0}$ is reduced by 2.1% and 1.0% in comparison to $M^{0}N^{0}S^{42}$ and $M^{5}N^{0}S^{0}$ respectively. This is due to the hybrid combination of macro and micro fibers.
- Hybrid fibers do not improve maximum crack width of microcracks, but more investigation is required to see their impact on macrocracks.

- Hybrid fibers at similar doses by volume outperform single fiber-reinforced mixes in terms of cracking area. $M^5N^{0.5}S^0$ outperforms $M^5N^0S^0$ and $M^0N^0S^{42}$ by 16.6% and 15.7% respectively.

Overall, the mix deemed best to reinforce as a hybrid combination of fibers is $M^5N^{0.5}S^0$. The following comparisons will be made to $M^5N^0S^0$, as improving this mix was one of the main objectives of this experiment. In regards to mechanical properties, it increased early age compressive strength by 14.8%, increased tensile strength at 28 days by 2.8%, and increased modulus of rupture by 3.5%. In addition, the cracking frequency is similarly improved. The number of cracks is reduced by 14.6%, the average crack width is reduced by 1.0%, and the cracking area is reduced by 15.7%. This can be attributed to a lower stress accumulation experienced in the rings from the implementation of micro fibers. The following illustrates future work that can be done to further improve the results found in this study

- Modify the AASHTO ring test by reducing the concrete width in order to induce full depth cracking of fiber-reinforced specimens. This way, age of cracking and maximum crack width parameters can be investigated.
- Implement the $M^5N^{0.5}S^0$ mix in the field to see if it can be pumped, poured, etc. The fresh properties of this hybrid combination recorded in the lab might not accurately represent how the mix will perform in the field.
- Since the control mix consisting of steel fibers performed better than the control mix consisting of macro fibers, perhaps the following hybrid combinations can be investigated:
    - $M^5N^0S^{42}$

- $M^{0}N^{0.5}S^{42}$

- In addition, perhaps hybrid combinations of all 3 types of fibers may be investigated. This includes $M^{2.5}N^{0.5}S^{21}$.

6. Bibliography

AASHTO Standard PP-34. Washington, D.C. “Estimating the Cracking Tendency of Concrete,” American Association of Highway and Transportation Officials, 2005.

AASHTO Standard T-277. Washington, D.C. “Standard Method of Test for Electrical Indication of Concrete’s Ability to Resist Chloride Ion Penetration,” American Association of Highway and Transportation Officials, 2015.

AASHTO Standard T-358. Washington, D.C. “Standard Method of Test for Surface Resistivity Indication of Concrete’s Ability to Resist Chloride Ion Penetration,” American Association of Highway and Transportation Officials, 2017.

Abu-Obeida, Adi, et al. “Utilization of Fiber Reinforced High Performance Concrete (FR-HPC) in Reconstructed Bridge Decks.” Transportation Research Board, Jan. 2019.

Abu-Obeidah, Adi, et al. “Application of the Maturity Method in Predicting Concrete Strength in Early Age (within 24 Hours).” Transportation Research Board, Jan. 2016.

Aïtcin Pierre-Claude. *High-Performance Concrete*. Taylor & Francis, 2004.

Alhozaimy, A.m., et al. “Mechanical Properties of Polypropylene Fiber Reinforced Concrete and the Effects of Pozzolanic Materials.” Cement and Concrete Composites, vol. 18, no. 2, 1996, pp. 85–92., doi:10.1016/0958-9465(95)00003-8.

Aly, T., et al. “Effect of Polypropylene Fibers on Shrinkage and Cracking of Concretes.” Materials and Structures, vol. 41, no. 10, 22 Jan. 2008, pp. 1741–1753., doi:10.1617/s11527-008-9361-2.

ASTM Standard C39. West Conshohocken, PA. "Standard Test Method for Compressive Strength of Cylindrical Concrete Specimens," ASTM International, 2018, DOI: 10.1520/C0039_C0039M-18, www.astm.org.

ASTM Standard C78. West Conshohocken, PA. "Standard Test Method for Flexural Strength of Concrete (Using Simple Beam with Third-Point Loading)," ASTM International, 2018, DOI: 10.1520/C0078_C0078M-18, www.astm.org.

ASTM Standard C157. West Conshohocken, PA." Standard Test Method for Length Change of Hardened Hydraulic-Cement Mortar and Concrete," ASTM International, 2017, DOI: 10.1520/C0157_C0157M-17, www.astm.org.

ASTM Standard C469. West Conshohocken, PA. "Standard Test Method for Static Modulus of Elasticity and Poisson's Ratio of Concrete in Compression," ASTM International, 2014, DOI: 10.1520/C0469_C0469M-14, www.astm.org.

ASTM Standard C496. West Conshohocken, PA. "Standard Test Method for Splitting Tensile Strength of Cylindrical Concrete Specimens," ASTM International, 2017, DOI: 10.1520/C0496_C0496M-17, www.astm.org.

Balaguru, P, and V Ramakrishnan. "Properties of Fiber Reinforced Concrete: Workability, Behavior Under Long-Term Loading, and Air-Void Characteristics." ACI Materials Journal, vol. 85, no. 3, 1988, doi:10.14359/1849.

Banthia, N. "Hybrid Fiber Reinforced Concrete (HyFRC): Fiber Synergy in High Strength Matrices." Materials and Structures, vol. 37, no. 274, 2004, pp. 707–716., doi:10.1617/14095.

Bentz, Dale P, and W Jason Weiss. "Internal Curing : A 2010 State-of-TheArt Review." 2011, doi:10.6028/nist.ir.7765.

Brewer, Gregory. “Restrained Shrinkage Behavior of High Performance Concrete Reinforced with Synthetic and Steel Fibers.” May 2018.

Burrows, Richard W. *The Visible and Invisible Cracking of Concrete*. American Concrete Institute, 1998.

Campione, Giuseppe, et al. “Seismic Behavior of Fibre Reinforced Concrete Frames.” *12 WCEE 2000*, Jan. 2010.

Cucchiara, Calogero, et al. “Effectiveness of Stirrups and Steel Fibres as Shear Reinforcement.” Cement and Concrete Composites, vol. 26, no. 7, 2004, pp. 777–786., doi:10.1016/j.cemconcomp.2003.07.001.

Eren, Özgür, and Tahir Çelik. “Effect of Silica Fume and Steel Fibers on Some Properties of High-Strength Concrete.” Construction and Building Materials, vol. 11, no. 7-8, 1997, pp. 373–382., doi:10.1016/s0950-0618(97)00058-5.

French, Catherine, et al. “Transverse Cracking in Concrete Bridge Decks.” Transportation Research Record: Journal of the Transportation Research Board, vol. 1688, no. 1, 1999, pp. 21–29., doi:10.3141/1688-03.

Ghanchi, Zeeshan. “Restrained Shrinkage Behavior of Polypropylene Fiber-Reinforced Self-Consolidating Concrete.” January 2015.

Grzybowski, Miroslaw, and Surendra P. Shah. “Shrinkage Cracking of Fiber Reinforced Concrete.” ACI Materials Journal, vol. 87, no. 2, 1990, doi:10.14359/1951.

Hasan, M.J., et al. “An Experimental Investigation on Mechanical Behavior of Macro Synthetic Fiber Reinforced Concrete .” International Journal of Civil & Environmental Engineering, vol. 11, no. 3, June 2011.

Hossain, Akhter B., and Jason Weiss. “Assessing Residual Stress Development and Stress Relaxation in Restrained Concrete Ring Specimens.” Cement and Concrete Composites, vol. 26, no. 5, 2004, pp. 531–540., doi:10.1016/s0958-9465(03)00069-6.

Hsie, Machine, et al. “Mechanical Properties of Polypropylene Hybrid Fiber-Reinforced Concrete.” Materials Science and Engineering: A, vol. 494, no. 1-2, 2008, pp. 153–157., doi:10.1016/j.msea.2008.05.037.

Jerga, Ján. “Physico-Mechanical Properties of Carbonated Concrete.” Construction and Building Materials, vol. 18, no. 9, 15 Apr. 2004, pp. 645–652., doi:10.1016/j.conbuildmat.2004.04.029.

Jiang, Chenhui, et al. “Autogenous Shrinkage of High Performance Concrete Containing Mineral Admixtures under Different Curing Temperatures.” Construction and Building Materials, vol. 61, 2014, pp. 260–269., doi:10.1016/j.conbuildmat.2014.03.023.

Khatri, R.P., et al. “Effect of Different Supplementary Cementitious Materials on Mechanical Properties of High Performance Concrete.” *Cement and Concrete Research*, vol. 25, no. 1, 1995, pp. 209–220., doi:10.1016/0008-8846(94)00128-l.

Kosmatka, Steve. “Concrete Technology Today.” Portland Cement Association, vol. 19, no. 1, Apr. 1998.

Marcos-Meson, Victor, et al. “Corrosion Resistance of Steel Fibre Reinforced Concrete - A Literature Review.” Cement and Concrete Research, vol. 103, 2018, pp. 1–20., doi:10.1016/j.cemconres.2017.05.016.

Mehta, P. Kumar. “High-Performance, High-Volume Fly Ash Concrete for Sustainable Development.” Jan. 2004.

Mehta, P. Kumar, and Paulo J. M. Monteiro. *Concrete: Microstructure, Properties, and Materials*. McGraw-Hill Education, 2014.

Nassif, Hani H., et al. "Effect of Pozzolanic Materials and Curing Methods on the Elastic Modulus of HPC." Cement and Concrete Composites, vol. 27, no. 6, 2005, pp. 661–670., doi:10.1016/j.cemconcomp.2004.12.005.

Passuello, Alexandra, et al. "Cracking Behavior of Concrete with Shrinkage Reducing Admixtures and PVA Fibers." Cement and Concrete Composites, vol. 31, no. 10, Aug. 2009, pp. 699–704., doi:10.1016/j.cemconcomp.2009.08.004.

Pigeon, Michel, et al. "Frost Resistant Concrete." *Construction and Building Materials*, vol. 10, no. 5, July 1996, pp. 339–348., doi:10.1016/0950-0618(95)00067-4.

Shen, Dejian, et al. "Tensile Creep and Cracking Resistance of Concrete with Different Water-to-Cement Ratios at Early Age." *Construction and Building Materials*, vol. 146, Aug. 2017, pp. 410–418., doi:10.1016/j.conbuildmat.2017.04.056.

Samad, S., and A. Shah. "Role of Binary Cement Including Supplementary Cementitious Material (SCM), in Production of Environmentally Sustainable Concrete: A Critical Review." International Journal of Sustainable Built Environment, vol. 6, no. 2, Dec. 2017, pp. 663–674., doi:10.1016/j.ijsbe.2017.07.003.

Song, P.s, and S Hwang. "Mechanical Properties of High-Strength Steel Fiber-Reinforced Concrete." Construction and Building Materials, vol. 18, no. 9, 2004, pp. 669–673., doi:10.1016/j.conbuildmat.2004.04.027.

Tazawa, Ei-Ichi, et al. "Chemical Shrinkage and Autogenous Shrinkage of Hydrating Cement Paste." *Cement and Concrete Research*, vol. 25, no. 2, Feb. 1995, pp. 288–292., doi:10.1016/0008-8846(95)00011-9.

Tazawa, Eiichi. *Autogenous Shrinkage of Concrete*. E & FN Spon, 1999.

Toutanji, H, et al. "Chloride Permeability and Impact Resistance of Polypropylene-Fiber-Reinforced Silica Fume Concrete." Cement and Concrete Research, vol. 28, no. 7, 1998, pp. 961–968., doi:10.1016/s0008-8846(98)00073-8.

Troxell, G.E. et al., Proc. *ASTM*, vol. 58, 1958; and ACI Monograph 6, 1971, pp.128, 151

Wafa, Faisal. "Properties & Applications of Fiber Reinforced Concrete." Journal of King Abdulaziz University-Engineering Sciences, vol. 2, no. 1, 1990, pp. 49–63., doi:10.4197/eng.2-1.4.

Wongtanakitcharoen, Thanasak, and Antoine E. Naaman. "Unrestrained Early Age Shrinkage of Concrete with Polypropylene, PVA, and Carbon Fibers." Materials and Structures, vol. 40, no. 3, 2006, pp. 289–300., doi:10.1617/s11527-006-9106-z.

Wu, Linmei, et al. "Autogenous Shrinkage of High Performance Concrete: A Review." *Construction and Building Materials*, vol. 149, 15 Sept. 2017, pp. 62–75.

Yao, Wu, et al. "Mechanical Properties of Hybrid Fiber-Reinforced Concrete at Low Fiber Volume Fraction." Cement and Concrete Research, vol. 33, no. 1, 2003, pp. 27–30., doi:10.1016/s0008-8846(02)00913-4.

Zollo, Ronald F. "Fiber-Reinforced Concrete: an Overview after 30 Years of Development." Cement and Concrete Composites, vol. 19, no. 2, 1997, pp. 107–122., doi:10.1016/s0958-9465(96)00046-7.